Research Square

Preprints are preliminary reports that have not undergone peer review.
They should not be considered conclusive, used to inform clinical practice,
or referenced by the media as validated information.

Chitosan-encapsulated α-lipoic acid enhances germination and alleviates salinity and drought stress in pea seedlings

Ibtisam A. M. Alghabban

e.algaban@ut.edu.sa

University College of Duba, University of Tabuk

Research Article

Keywords: α-lipoic acid, Chitosan nanoparticles, Seed priming, Salinity stress, Drought stress, Antioxidant defense system

Posted Date: November 24th, 2026

DOI: https://doi.org/10.21203/rs.3.rs-11543823/v1

License: This work is licensed under a Creative Commons Attribution 4.0 International License.
Read Full License

Additional Declarations: No competing interests reported.

Chitosan-encapsulated α-lipoic acid enhances germination and alleviates salinity and drought stress in pea seedlings

Ibtisam A. M. Alghabban

Department of Biology, University College of Duba, University of Tabuk, Tabuk, Saudi Arabia; e.algaban@ut.edu.sa

Abstract

Salinity and drought impair seed germination and early seedling establishment by disrupting redox balance, membrane integrity, and nutrient homeostasis. This study investigated whether seed priming with α-lipoic acid encapsulated in chitosan nanoparticles (Ch-ALA-NPs) could improve pea (*Pisum sativum* L.) responses to these stresses. The nanoparticles had a mean hydrodynamic diameter of 148.7 ± 7.3 nm, a zeta potential of +28.9 ± 1.7 mV, an encapsulation efficiency of 78.4 ± 3.2%, and a loading capacity of 12.6 ± 1.1%. Seven treatments comprised non-primed and hydroprimed controls, salinity and drought controls, and Ch-ALA-NP priming under non-stress, salinity, and drought conditions. Final germination following Ch-ALA-NP priming reached 100% under non-stress conditions, 96.67% under salinity, and 85.00% under drought, compared with 76.67% and 68.33% in the corresponding salinity and drought controls. Priming increased antioxidant enzyme activities, including APX, CAT, GPX, GR, and SOD; APX activity reached 44.60 and 42.79 U g^{-1} min^{-1} FW under salinity and drought, respectively. These responses were accompanied by lower H_2O_2 accumulation, lipid peroxidation, electrolyte leakage, and Na^+ accumulation, together with greater proline accumulation and retention of P, N, Ca, Fe, Zn, Mn, and Cu. Ch-ALA-NP priming also altered the expression of stress-responsive genes, including *LEA*, *PsbD*, *PDH45*, *ABR1*, aquaporin, *HSP70*, and *OSM34*. Particularly pronounced induction was observed for *PDH45* and *OSM34* under drought and for *LEA* and *HSP70* under salinity. Overall, Ch-ALA-NP priming improved germination and physiological responses to salinity and drought in pea seedlings, with accompanying changes in antioxidant activity, osmotic adjustment, nutrient status, membrane integrity, and stress-responsive gene expression. These findings support further evaluation of Ch-ALA-NPs as a seed-priming treatment for improving pea establishment under abiotic stress.

Keywords; α-lipoic acid, Chitosan nanoparticles, Seed priming, Salinity stress, Drought stress, Antioxidant defense system

Introduction

Salinity and drought are among the most pervasive abiotic stresses limiting agricultural productivity worldwide. These stresses are particularly detrimental during seed germination and early seedling establishment, stages that are highly sensitive to environmental perturbations (Aqaei et al. 2020; Weisany and Khosropour 2023). Osmotic imbalance, ionic toxicity, and excessive generation of reactive oxygen species (ROS) collectively disrupt cellular metabolism, delay radicle protrusion, and impair stand establishment in legumes (Sharma et al. 2021). In pea (*Pisum sativum* L.), a crop valued for its nutritional and agronomic importance, early-stage stress sensitivity frequently results in poor emergence and reduced yield potential under suboptimal soil conditions.

A central consequence of both salinity and drought is oxidative stress. Rapid reactivation of mitochondrial respiration during imbibition leads to ROS production, including superoxide radicals ($O_2^{-\bullet}$) and hydrogen peroxide (H_2O_2) (Manvelian et al. 2021). Under stress, restricted water uptake and ionic imbalance further amplify ROS generation beyond the scavenging capacity of the endogenous antioxidant system (Ahanger et al. 2017). Excess ROS trigger lipid peroxidation, protein oxidation, membrane destabilization, and impairment of photosynthetic machinery (El-Beltagi and Mohamed 2013). Although plants possess enzymatic antioxidant defenses such as superoxide dismutase (SOD), catalase (CAT), ascorbate peroxidase (APX), glutathione reductase (GR), guaiacol peroxidase (GPX), and monodehydroascorbate reductase (MDHAR) their activation is often insufficient to fully counteract stress-induced oxidative damage during early development (Rao et al. 2025).

Seed priming has emerged as a promising strategy to enhance stress tolerance by preconditioning metabolic and defense pathways before stress exposure (Marthandan et al. 2020). Priming treatments accelerate germination kinetics, improve redox balance, and promote osmotic adjustment. Among bioactive compounds used in priming, α-lipoic acid (ALA) is gaining attention due to its dual antioxidant properties (Mian et al. 2024). ALA and its reduced form, dihydrolipoic acid, function as potent redox modulators capable of directly scavenging ROS and regenerating other antioxidants, including ascorbate and glutathione (Tripathi et al. 2023). Additionally, ALA participates in mitochondrial energy metabolism and may influence stress-related gene expression

and signaling pathways. However, ALA is poorly water-soluble and susceptible to degradation, limiting its stability and bioavailability when applied directly (Wang et al. 2025).

Nanotechnology-based delivery systems offer a solution to these limitations. Chitosan, a biodegradable and biocompatible polysaccharide derived from chitin, is widely used as a nanocarrier due to its cationic nature, film-forming ability, and intrinsic bioactivity (Jin et al. 2021). Chitosan nanoparticles prepared via ionic gelation provide controlled release, enhanced stability, and improved cellular interaction of encapsulated compounds (Soufiani et al. 2025). The positive surface charge of chitosan nanoparticles facilitates interaction with negatively charged plant cell membranes, potentially enhancing uptake efficiency (Nandini et al. 2025). Encapsulation of ALA within chitosan nanoparticles may therefore improve its solubility, protect it from premature degradation, and allow sustained release during the critical phases of germination and early growth.

Beyond biochemical protection, effective stress mitigation also requires maintenance of ionic homeostasis and activation of molecular defense pathways. Under salinity, excessive Na^+ disrupts K^+ balance and interferes with nutrient acquisition, while drought limits water transport and nutrient mobility (Weisany et al. 2024). Osmoprotectants such as proline and stress-related proteins including late embryogenesis abundant (LEA) proteins, heat shock proteins (HSP70), aquaporins, helicases (PDH45), ABA-responsive regulators (ABR1), and osmotin-like proteins (OSM34) play key roles in osmotic adjustment, protein stabilization, and stress signaling. A strategy that integrates redox regulation, ionic balance, osmoprotection, and transcriptional activation is therefore essential for robust early-stage tolerance (Sackey et al. 2025).

In this context, we hypothesized that chitosan-encapsulated α-lipoic acid (nano-ALA) could function as an integrative nano-priming agent capable of enhancing germination performance and early stress resilience in pea. The objectives of this study were: (i) to formulate and physicochemically characterize ALA-loaded chitosan nanoparticles; (ii) to evaluate their effects on germination dynamics under salinity and drought stress; and (iii) to elucidate the associated biochemical and molecular mechanisms, focusing on antioxidant enzyme systems, oxidative stress markers, ionic homeostasis, osmolyte accumulation, and stress-responsive gene expression.

Material and methods

Preliminary optimization of ALA concentration

Prior to the main greenhouse experiment, a preliminary germination assay was conducted to optimize the concentration of α-lipoic acid (ALA) used for seed priming. The optimization was performed in two sequential stages. In the initial screening, uniform and surface-sterilized *Pisum sativum* seeds were exposed to a broad range of ALA concentrations (1, 2, 4, 8, 16, and 22 mM) together with a distilled-water control. This preliminary range was used to evaluate the general concentration-dependent response of pea seeds to ALA and to identify concentrations associated with growth inhibition or potential phytotoxicity. Based on the responses observed during this initial screening and considering the greater physiological suitability of lower ALA concentrations, a second optimization assay was conducted using 0.1, 0.2, 0.5, and 1.0 mM ALA, along with a distilled-water control.

For both screening stages, sterilized seeds were soaked in the respective ALA solutions for 48 h under controlled laboratory conditions. After priming, seeds were removed from the solutions, gently blotted with sterile filter paper, and transferred to sterile Petri dishes lined with moistened filter paper. Each treatment consisted of three biological replicates, with an equal number of seeds per replicate, and treatments were arranged in a completely randomized design. The Petri dishes were maintained under controlled conditions, and germination was assessed based on visible radicle emergence. Germination percentage, radicle length, plumule length, and overall seedling vigor were recorded to determine the most effective ALA concentration.

Among the low-dose treatments evaluated in the second screening, 0.2 mM ALA produced the most consistent improvement in germination performance and early seedling growth without detectable phytotoxic effects. Higher concentrations did not provide additional benefits and, particularly within the initial broad-range screening, tended to reduce early seedling performance. Therefore, 0.2 mM ALA was selected as the optimum concentration for the subsequent greenhouse experiment. The selected ALA concentration was subsequently incorporated into chitosan nanoparticles through ionic gelation to produce ALA-loaded chitosan nanoparticles (Ch-ALA-NPs). Thus, the Ch-ALA-NP priming formulation applied in the main experiment contained an ALA-equivalent concentration of 0.2 mM.

Experimental treatments and sampling

The main greenhouse experiment comprised seven treatment groups arranged in a randomized complete block design (RCBD) with three biological replicates (n = 3). The treatments included CNP, control non-primed dry seeds grown under non-stress conditions; CHP, hydroprimed seeds grown under non-stress conditions; NCS, hydroprimed seeds exposed to salinity stress; NCD, hydroprimed seeds exposed to drought stress; AlpP, seeds primed with Ch-ALA-NPs containing an ALA-equivalent concentration of 0.2 mM and grown under non-stress conditions; AlpPS, Ch-ALA-NP-primed seeds exposed to salinity stress; and AlpPD, Ch-ALA-NP-primed seeds exposed to drought stress. Salinity and drought treatments were imposed five days after germination and maintained for 14 days. At the end of the stress period (22 days after sowing), seedlings were carefully harvested and analyzed for growth, physiological, biochemical, and molecular attributes to evaluate the effectiveness of Ch-ALA-NP seed priming in alleviating salinity- and drought-induced stress in *P. sativum* (Fig 1).

Physicochemical characterization of chitosan nanoparticles and ALA-loaded nanoparticles

Dynamic Light Scattering (DLS) and Zeta Potential

The hydrodynamic diameter, polydispersity index (PDI), and surface charge (zeta potential) of blank chitosan nanoparticles (ChN) and α-lipoic acid–loaded nanoparticles (ChAN) were determined using a Zetasizer Nano ZS (Malvern Instruments, UK) equipped with a 633 nm He–Ne laser. Prior to measurements, freshly prepared nanoparticle suspensions were diluted (1:50–1:100) with deionized water to avoid multiple scattering effects and to obtain an appropriate count rate. Particle size and PDI were measured at 25 °C using a scattering angle of 173° (backscatter mode). Zeta potential was determined by electrophoretic light scattering in folded capillary cells at 25 °C. Each sample was analyzed in triplicate, and results are presented as mean ± standard error.

where $ALA_{total}$is the initial amount of ALA added during formulation, $ALA_{free}$is the amount detected in the supernatant, and nanoparticle mass refers to the dry weight of the collected nanoparticles.

X-ray Diffraction (XRD)

The crystalline structure of ChN and ChAN was examined using an X-ray diffractometer (PANalytical X'Pert Pro or equivalent) operating with Cu Kα radiation (λ = 1.5406 Å), at 40 kV and 30 mA. Freeze-dried samples were mounted on a sample holder and scanned over a 2θ range of 5–80° at a step size of 0.02° and a scanning speed of 2° min^{-1}. Diffraction patterns were used to evaluate changes in crystallinity after ALA loading, and peak broadening/intensity reduction was interpreted as evidence of polymer–drug interaction and increased amorphous character.

Fourier Transform Infrared Spectroscopy (FTIR)

Functional groups and molecular interactions between chitosan, TPP, and ALA were analyzed by FTIR spectroscopy using an FTIR spectrometer (Bruker Tensor 27, Germany). Freeze-dried samples were mixed with KBr and pressed into pellets (or measured using ATR mode). Spectra were recorded in the range of 4000–400 cm^{-1} with a resolution of 4 cm^{-1} and 32 scans per sample. Characteristic chitosan bands (O–H/N–H, amide I/II, C–O–C) were compared with ChAN to identify peak shifts and the appearance of ALA-specific absorption bands, indicating successful encapsulation and intermolecular interactions.

Encapsulation of ALA into Chitosan Nanoparticles

α-Lipoic acid (ALA) was incorporated into chitosan nanoparticles via the ionic gelation technique. Briefly, a 0.25% (w/v) chitosan solution was prepared by dissolving low–molecular weight chitosan (degree of deacetylation ≈ 90%) in 2% (v/v) acetic acid under continuous magnetic stirring at room temperature for 12 h to ensure complete solubilization. The pH was subsequently adjusted to 4.5 using 0.1 M NaOH to facilitate optimal nanoparticle formation. Sodium tripolyphosphate (TPP) was prepared separately in deionized water at a concentration of 0.25 mg mL^{-1} and used as a cross-linking agent (Quester et al. 2022).

For nanoparticle formation, an ALA solution (6 mg mL^{-1} prepared in 20% ethanol) was introduced dropwise into the chitosan solution under constant stirring at 800 rpm. After 15 min of homogenization, the TPP solution was added dropwise to the chitosan–ALA mixture at the same stirring speed to induce nanoparticle formation through electrostatic interactions between the positively charged amino groups of chitosan and the negatively charged phosphate groups of TPP. The reaction mixture was maintained under continuous stirring for 2 h at room temperature to

ensure complete cross-linking and stabilization. The nanoparticle suspension was then centrifuged at 10,000 × g for 30 min at 4 °C. The resulting pellet was washed three times with deionized water to remove any unencapsulated ALA and residual reagents. The purified ChAN were subsequently freeze-dried and stored at −20 °C in sealed containers until further characterization and use in seed priming experiments.

Germination Characteristics

Germination assays were conducted under controlled laboratory conditions to evaluate the effects of nano-ALA priming and stress treatments on pea seed performance. Seeds were surface sterilized in 1% sodium hypochlorite for 5 min and thoroughly rinsed with distilled water. Priming treatments included hydropriming (soaking in distilled water for 12 h) and nano-ALA priming using α-lipoic acid encapsulated in chitosan nanoparticles, followed by drying to original moisture content. Salinity stress was imposed using NaCl solution (100 mM), while drought stress was simulated using polyethylene glycol (PEG-6000) adjusted to an osmotic potential of approximately −0.5 MPa, following Michel and Kaufmann (1973). Germination was performed in Petri dishes lined with moistened filter paper at 25 ± 1°C in a growth chamber. Germination was recorded daily for 10 days, and final germination percentage (FGP), mean germination time (MGT), time to 50% germination (T50), and germination index (GI) were calculated according to standard procedures described by Ellis and Roberts (1981) (Ellis and Roberts 1981).

Antioxidant Enzyme Extraction

Fresh seedling tissues (0.5 g) were harvested and immediately homogenized in 5 mL of ice-cold extraction buffer consisting of 50 mM potassium phosphate buffer (pH 7.0), 1 mM ethylenediaminetetraacetic acid (EDTA), and 1% (w/v) polyvinylpyrrolidone (PVP). The phosphate buffer maintained physiological pH stability, while EDTA chelated divalent metal ions that could catalyze non-enzymatic oxidative reactions. PVP was included to bind phenolic compounds and prevent their interference with enzyme activity. Homogenization was performed under chilled conditions to minimize enzymatic degradation and proteolysis. The homogenate was centrifuged at 12,000 × g for 20 min at 4 °C, and the clear supernatant was carefully collected as

the crude enzyme extract. All extraction steps were carried out at 0–4 °C to preserve enzymatic integrity. The obtained extract was immediately used for antioxidant enzyme assays. Total soluble protein content was quantified using the Bradford (1976) method, based on Coomassie Brilliant Blue G-250 dye binding to protein molecules, with bovine serum albumin (BSA) used as the standard (Bradford 1976). Enzyme activities were normalized to fresh weight (FW) and, where appropriate, to protein content.

Catalase (CAT; EC 1.11.1.6)

Catalase activity was determined according to Aebi (1984) by monitoring the decomposition rate of hydrogen peroxide (H_2O_2). The reaction mixture (3 mL final volume) contained 50 mM potassium phosphate buffer (pH 7.0), 10–15 mM H_2O_2, and an appropriate volume of enzyme extract. The decrease in absorbance was recorded at 240 nm for 1 min using a UV–Vis spectrophotometer. The activity was calculated using the extinction coefficient of H_2O_2 (39.4 mM^{-1} cm^{-1}) and expressed as units (U) per gram fresh weight (U g^{-1} FW), where one unit corresponds to the amount of enzyme decomposing 1 µmol of H_2O_2 per minute (Aebi 1984).

Superoxide Dismutase (SOD; EC 1.15.1.1)

SOD activity was measured following Beauchamp and Fridovich (1971), based on its ability to inhibit the photochemical reduction of nitroblue tetrazolium (NBT). The reaction mixture contained 50 mM phosphate buffer (pH 7.8), 13 mM methionine, 75 µM NBT, 2 µM riboflavin, 0.1 mM EDTA, and enzyme extract. The reaction was initiated under fluorescent light (≈4000 lux) for 10–15 min. Absorbance was measured at 560 nm. One unit of SOD activity was defined as the amount of enzyme required to cause 50% inhibition of NBT reduction compared to a control without enzyme extract. Results were expressed as U g^{-1} FW. SOD represents the first line of antioxidant defense by catalyzing the dismutation of superoxide radicals ($O_2^{-}\bullet$) into H_2O_2 and O_2 (Beauchamp and Fridovich 1971).

Glutathione Reductase (GR; EC 1.6.4.2)

GR activity was assayed according to Foyer and Halliwell (1976) by monitoring the oxidation of NADPH at 340 nm. The reaction mixture contained 50 mM phosphate buffer (pH 7.5), 0.5 mM oxidized glutathione (GSSG), 0.12 mM NADPH, and enzyme extract in a total volume of 3 mL. The decrease in absorbance at 340 nm was recorded for 1 min. Activity was calculated using the extinction coefficient of NADPH (6.22 mM^{-1} cm^{-1}) and expressed as U g^{-1} FW. GR is a key enzyme in the ascorbate–glutathione cycle, maintaining the reduced glutathione (GSH) pool necessary for cellular redox homeostasis (Foyer and Halliwell 1976).

Ascorbate Peroxidase (APX; EC 1.11.1.11)

APX activity was determined following Nakano and Asada (1981). The reaction mixture consisted of 50 mM potassium phosphate buffer (pH 7.0), 0.5 mM ascorbate, 0.1 mM H_2O_2, and enzyme extract. The reaction was initiated by adding H_2O_2, and the decrease in absorbance due to ascorbate oxidation was monitored at 290 nm for 1 min (Nakano and Asada 1981). Activity was calculated using the extinction coefficient of ascorbate (2.8 mM^{-1} cm^{-1}) and expressed as U g^{-1} FW. APX is a major component of the ascorbate–glutathione cycle and plays a crucial role in fine-tuning intracellular H_2O_2 levels, particularly in chloroplasts.

Guaiacol Peroxidase (GPX; EC 1.11.1.7)

Guaiacol peroxidase activity was measured according to Chance and Maehly (1955). The reaction mixture contained 50 mM phosphate buffer (pH 6.0), 20 mM guaiacol, 10 mM H_2O_2, and enzyme extract in a final volume of 3 mL (Chance and Maehly 1955). The formation of tetraguaiacol was monitored spectrophotometrically at 470 nm for 1 min. Activity was calculated using the extinction coefficient of tetraguaiacol (26.6 mM^{-1} cm^{-1}) and expressed as U g^{-1} FW. GPX contributes to peroxidative detoxification processes and is often associated with cell wall strengthening and stress-induced oxidative metabolism.

Monodehydroascorbate Reductase (MDHAR)

MDHAR activity was determined following the method of Arrigoni et al. (1981), based on monitoring the oxidation rate of NADH at 340 nm. The reaction mixture (final volume 3 mL) contained 50 mM potassium phosphate buffer (pH 7.0), 0.2 mM NADH, 2.5 mM ascorbate, 0.5 U ascorbate oxidase, and an appropriate volume of enzyme extract (Arrigoni et al. 1981). The reaction was initiated by the addition of ascorbate oxidase, which catalyzes the oxidation of ascorbate to MDHA. MDHAR subsequently reduces MDHA back to ascorbate using NADH as an electron donor, resulting in NADH oxidation. The decrease in absorbance at 340 nm, corresponding to NADH oxidation, was recorded spectrophotometrically for 1 min. Enzyme activity was calculated using the extinction coefficient of NADH (6.22 mM^{-1} cm^{-1}) and expressed as units per gram fresh weight (U g^{-1} FW), where one unit represents the oxidation of 1 µmol NADH per minute.

Mineral Nutrient Analysis

For mineral nutrient determination, seedling samples were harvested, thoroughly washed with distilled water to remove surface contaminants, and oven-dried at 70 °C until constant weight was achieved. The dried samples were finely ground using a stainless-steel mill and passed through a fine mesh sieve to ensure homogeneity prior to chemical analysis. For macro- and micronutrient extraction, approximately 0.5 g of ground plant material was subjected to wet digestion using a mixture of concentrated nitric acid (HNO_3) and perchloric acid ($HClO_4$) under controlled heating until a clear solution was obtained. After cooling, the digest was filtered and diluted to a known final volume with deionized water.

Sodium (Na^+) and potassium (K^+) concentrations were measured using a flame photometer according to the method of Chapman and Pratt (1961). Calibration curves were prepared using standard Na and K solutions, and results were expressed on a dry weight (DW) basis (Pratt and Chapman 1961).

Total nitrogen (N) content was determined using the Kjeldahl digestion–distillation method (Bremner, 1960). Briefly, organic nitrogen was converted to ammonium sulfate through acid digestion, followed by alkalization, distillation, and titration to quantify nitrogen concentration (Bremner 1965). Phosphorus (P) content was determined colorimetrically using the molybdenum

blue method described by Murphy and Riley (1962). In this method, inorganic phosphate reacts with ammonium molybdate under acidic conditions to form a phosphomolybdate complex, which is subsequently reduced to produce a blue-colored compound measured spectrophotometrically at 882 nm (Murphy and Riley 1962).

Calcium (Ca), iron (Fe), zinc (Zn), manganese (Mn), and copper (Cu) were quantified using atomic absorption spectrophotometry (AAS) following the standard procedures outlined by Allen et al. (1986). Appropriate hollow cathode lamps were used for each element, and calibration curves were established using certified standard solutions. All measurements were performed in triplicate, and concentrations were expressed as μmol g^{-1} DW or mg kg^{-1} DW as appropriate (Allen et al. 1998).

Malondialdehyde (MDA)

MDA content was quantified as an indicator of lipid peroxidation following the thiobarbituric acid (TBA) reaction method described by Heath and Packer (1968). Approximately 0.5 g of fresh seedling tissue was homogenized in 5 mL of 0.1% (w/v) trichloroacetic acid (TCA) and centrifuged at 10,000 × g for 10 min. An aliquot of the supernatant was mixed with 0.5% (w/v) TBA prepared in 20% TCA and heated at 95 °C for 30 min (Heath and Packer 1968). The reaction was terminated by rapid cooling in an ice bath, followed by centrifugation to clarify the solution. Absorbance was measured at 532 nm and corrected for nonspecific turbidity at 600 nm. MDA concentration was calculated using the extinction coefficient of 155 mM^{-1} cm^{-1} and expressed as nmol g^{-1} FW.

Hydrogen Peroxide (H_2O_2)

Hydrogen peroxide content was determined according to Velikova et al. (2000) based on potassium iodide (KI) reaction. Fresh tissue (0.5 g) was homogenized in cold 0.1% (w/v) TCA and centrifuged at 12,000 × g for 15 min at 4 °C. The reaction mixture consisted of supernatant, 10 mM potassium phosphate buffer (pH 7.0), and 1 M KI solution (Velikova et al. 2000). After incubation in the dark for 1 h, absorbance was measured at 390 nm. H_2O_2 concentration was calculated using a standard curve prepared with known H_2O_2 concentrations and expressed as μmol g^{-1} FW.

Electrolyte Leakage (EL)

Electrolyte leakage was assessed following Dionisio-Sese and Tobita (1998) to evaluate membrane stability and permeability. Leaf discs (or seedling segments) were rinsed with deionized water to remove surface-adhered ions and then incubated in test tubes containing a defined volume of deionized water (Dionisio-Sese and Tobita 1998). After incubation at room temperature for 24 h, the initial electrical conductivity (EC_1) of the solution was measured using a conductivity meter. Samples were subsequently autoclaved at 121 °C for 20 min to completely disrupt cellular membranes and release all electrolytes. After cooling to room temperature, final conductivity (EC_2) was measured. Electrolyte leakage was calculated as:

$$EL(\%) = \frac{EC_1}{EC_2} \times 100$$

Proline Content

Free proline accumulation was determined according to Bates et al. (1973) using the acid ninhydrin method. Approximately 0.5 g of dried plant material was homogenized in 3% (w/v) sulfosalicylic acid and filtered. The filtrate was reacted with acid ninhydrin solution and glacial acetic acid in a boiling water bath for 1 h. The reaction was terminated on ice, and proline was extracted with toluene (Bates et al. 1973). The chromophore-containing toluene phase was measured spectrophotometrically at 520 nm. Proline concentration was calculated using a standard curve prepared with L-proline and expressed as μmol g^{-1} DW.

Gene Expression Analysis

Total RNA was isolated from fresh seedling tissues using a commercial plant RNA extraction kit according to the manufacturer's protocol, with particular care taken to prevent RNA degradation. Approximately 100 mg of frozen plant tissue was ground in liquid nitrogen to a fine powder prior to extraction. The integrity and purity of the extracted RNA were evaluated spectrophotometrically

by measuring absorbance ratios at A260/A280 and A260/A230 using a NanoDrop spectrophotometer. RNA quality was further verified by electrophoresis on 1% (w/v) agarose gel to confirm the presence of intact 28S and 18S rRNA bands without degradation.

To eliminate potential genomic DNA contamination, RNA samples were treated with RNase-free DNase I prior to cDNA synthesis. First-strand cDNA was synthesized from 1 µg of total RNA using a reverse transcription kit with oligo(dT) primers, following the manufacturer's instructions. The resulting cDNA was diluted appropriately and stored at −20 °C until further analysis.

Quantitative real-time PCR (qRT-PCR) was carried out using SYBR Green master mix in a real-time PCR system under optimized cycling conditions (initial denaturation followed by 40 amplification cycles). Each reaction contained SYBR Green mix, gene-specific forward and reverse primers, diluted cDNA template, and nuclease-free water in a final volume of 20 µL. Amplification specificity was confirmed by melting curve analysis to ensure the absence of primer dimers or nonspecific products.

Relative gene expression levels were calculated using the comparative Ct ($2^{-}\Delta\Delta Ct$) method described by Livak and Schmittgen (2001), with actin serving as the internal reference gene for normalization. Each biological sample was analyzed in three independent biological replicates with three technical replicates per reaction to ensure reproducibility and accuracy (Livak and Schmittgen 2001).

Statistical Analysis

All experiments were conducted using a completely randomized design (CRD) with three independent biological replicates per treatment. Data are presented as mean ± standard error (SE). Prior to statistical evaluation, datasets were examined for normality and homogeneity of variance using Shapiro–Wilk and Levene's tests, respectively. When necessary, percentage data were arcsine square-root transformed to satisfy the assumptions of parametric analysis. Differences among treatments were analyzed using two-way analysis of variance for germination, biochemical, and molecular parameters. For experiments involving stress and priming factors, two-way ANOVA was performed to assess the main effects and their interaction. When significant differences were detected ($p \leq 0.05$), means were separated using the least significant difference (LSD) test at the

5% probability level. All statistical analyses were performed using statistical software (SAS 9.1 software), and graphical representations were prepared using appropriate plotting tools. Gene expression data obtained from qRT-PCR were analyzed based on ΔCt values prior to relative quantification ($2^{-}\Delta\Delta Ct$ method), and statistical comparisons were conducted on log-transformed expression ratios when required to ensure variance homogeneity.

Results

Physicochemical characterization of Ch-NPs and Ch-ALA-NPs

The physicochemical characteristics of Ch-NPs and Ch-ALA-NPs were evaluated using DLS, XRD, and FTIR (Fig. 2). Incorporation of ALA into the chitosan nanoparticles increased particle size, slightly broadened the particle-size distribution, reduced the positive surface charge and crystallinity, and produced characteristic changes in the FTIR spectrum, supporting the successful incorporation of ALA into the chitosan nanoparticle matrix.

The XRD pattern of Ch-NPs displayed characteristic diffraction features at $2\theta = 10.2°$ and 20.1°, confirming the semi-crystalline nature of chitosan nanoparticles (Fig 2A). In contrast, Ch-ALA-NPs exhibited a broader and less intense diffraction feature centered at approximately 20.0°, accompanied by attenuation of the characteristic low-angle peak. These changes indicate a reduction in the ordered crystalline domains following ALA incorporation. Consistent with this observation, the estimated crystallite size decreased from 22.4 nm in Ch-NPs to 18.7 nm in Ch-ALA-NPs. The broadening of the diffraction pattern and reduction in crystallite size suggest that incorporation of ALA disrupted intermolecular ordering within the chitosan matrix and promoted a comparatively more amorphous nanoparticle structure.

The FTIR spectrum of Ch-NPs showed a broad absorption band at 3425 cm^{-1}, attributed to overlapping O–H and N–H stretching vibrations, together with bands at 2875 cm^{-1} corresponding to C–H stretching, 1655 cm^{-1} assigned to amide I (C=O stretching), 1589 cm^{-1} associated with amide II/N–H bending, and 1074 cm^{-1} corresponding to C–O–C stretching of the polysaccharide backbone (Fig 2B). Following ALA incorporation, the broad O–H/N–H band shifted slightly to 3418 cm^{-1}, while the C–H stretching band appeared at 2872 cm^{-1}. Moreover, the amide I and amide II bands shifted from 1655 to 1648 cm^{-1} and from 1589 to 1578 cm^{-1}, respectively. Importantly,

Ch-ALA-NPs displayed an additional characteristic absorption band at 1715 cm^{-1}, attributed to the carbonyl (C=O) group of ALA. The C–O–C band also shifted slightly from 1074 to 1070 cm^{-1}. Collectively, the appearance of the ALA-associated carbonyl band and the shifts in the O–H/N–H and amide-related bands provide evidence of molecular interactions between ALA and the chitosan matrix, most plausibly through hydrogen bonding and electrostatic interactions, and further support successful ALA loading into the nanoparticles.

Ch-NPs exhibited a mean hydrodynamic diameter of 112.4 ± 5.6 nm, whereas loading with ALA increased the particle size to 148.7 ± 7.3 nm. The polydispersity index increased from 0.182 ± 0.014 for Ch-NPs to 0.231 ± 0.019 for Ch-ALA-NPs. Nevertheless, both PDI values remained relatively low, indicating a comparatively narrow and homogeneous particle-size distribution. The zeta potential of unloaded Ch-NPs was strongly positive (+34.6 ± 2.1 mV), consistent with the presence of protonated amino groups of chitosan. Following ALA incorporation, the zeta potential decreased to +28.9 ± 1.7 mV, suggesting partial interaction or masking of positively charged amino groups by the incorporated ALA. Ch-ALA-NPs showed an encapsulation efficiency of 78.4 ± 3.2% and a loading capacity of 12.6 ± 1.1%, demonstrating effective incorporation of ALA into the chitosan-based carrier system (Fig 2C).

EE%, LC%, and zeta potential analyses further confirmed the successful incorporation of α-lipoic acid (ALA) into chitosan nanoparticles. The formulated Ch-ALA-NPs exhibited an encapsulation efficiency of 78.4 ± 3.2%, indicating that most of the initially added ALA was effectively entrapped within the chitosan matrix. The loading capacity was 12.6 ± 1.1%, showing that ALA represented a substantial fraction of the total nanoparticle mass. In addition, the zeta potential decreased from +34.6 ± 2.1 mV for Ch-NPs to +28.9 ± 1.7 mV for Ch-ALA-NPs following ALA incorporation. The positive surface charge of both formulations is attributable to protonated amino groups of chitosan, whereas the reduction in zeta potential after ALA loading suggests partial neutralization or masking of these positively charged groups through interactions with ALA. Importantly, the Ch-ALA-NPs retained a relatively high positive zeta potential, indicating satisfactory colloidal stability and a reduced tendency toward particle aggregation. Collectively, the 78.4% encapsulation efficiency, 12.6% loading capacity, and +28.9 mV zeta potential demonstrate efficient ALA incorporation and favorable physicochemical stability of the chitosan nanocarrier, supporting its potential use for controlled ALA delivery in seed-priming applications.

Germination Characteristics

Significant differences were observed among treatments for all germination parameters ($p \leq 0.05$) (Fig. 3). Final germination percentage (FGP) was highest in AlpP (100%), followed by AlphSP, CHP, and CNP, which did not differ significantly from each other. In contrast, stress treatments markedly reduced germination, with the lowest FGP recorded in NCD (68.33%), followed by NCS (76.67%). Priming with α-lipoic acid nanoparticles under stress conditions (AlphSP and AlphDP) significantly improved FGP compared with their respective stress controls. The time required to reach 50% germination (T50) was significantly reduced in AlpP (3.33 days), indicating accelerated germination. Stress treatments, particularly NCS and CNP, exhibited the highest T50 values (5.0–5.67 days). Mean germination time (MGT) followed a similar trend, with AlpP showing the lowest MGT (2.63 days), while NCS and NCD exhibited the highest values (3.87 and 3.77 days, respectively). The germination index (GI) was significantly enhanced by priming, with AlpP recording the highest value (5.07). Stress conditions reduced GI, particularly in NCD (3.33). Notably, AlphSP and AlphDP treatments partially restored GI under salinity and drought stress.

Antioxidant Enzyme Activities

Nano-ALA priming markedly modified antioxidant enzyme activities in pea seedlings under both non-stress and stress conditions (Fig. 4A–F). In general, salinity and drought increased the activities of several antioxidant enzymes, while chitosan-encapsulated ALA priming further strengthened these responses. The magnitude of the effect varied among individual enzymes and stress conditions.

Catalase (CAT)

CAT activity differed significantly among treatments (Fig. 4A). The highest activity under non-stress conditions was observed in AlpP (0.91 ± 0.02 U g^{-1} min^{-1} FW), which was approximately 2.33-fold higher than that of CNP (0.39 ± 0.02 U g^{-1} min^{-1} FW). Salinity and drought alone increased CAT activity to 0.58 ± 0.02 and 0.64 ± 0.02 U g^{-1} min^{-1} FW in NCS and NCD, respectively. Nano-ALA priming further increased CAT activity under both stresses, reaching 0.73 ± 0.02 U g^{-1} min^{-1} FW in AlpPS and 0.82 ± 0.02 U g^{-1} min^{-1} FW in AlpPD, corresponding to increases of approximately 25.9% and 28.1% relative to their respective stress controls. CHP

showed relatively low CAT activity (0.42 ± 0.02 U g^{-1} min^{-1} FW), comparable with the non-primed control.

Superoxide dismutase (SOD)

SOD activity increased significantly in response to both salinity and drought stress (Fig. 4B). Compared with CNP (2.40 ± 0.06 U g^{-1} min^{-1} FW), SOD activity increased to 2.55 ± 0.06 in NCS and 2.63 ± 0.05 U g^{-1} min^{-1} FW in NCD. The greatest activities were recorded in AlpPD (2.83 ± 0.06) and AlpPS (2.76 ± 0.05 U g^{-1} min^{-1} FW), which were statistically similar and significantly higher than their corresponding stress controls. Nano-ALA priming increased SOD activity by approximately 8.2% under salinity and 7.6% under drought compared with NCS and NCD, respectively. By contrast, AlpP, CHP, and CNP showed similarly lower SOD activities under non-stress conditions.

Glutathione reductase (GR)

GR activity exhibited a pronounced stress-dependent response (Fig. 4C). The lowest value was recorded in CNP (1.97 ± 0.04 U g^{-1} min^{-1} FW), whereas salinity and drought increased GR activity to 3.34 ± 0.05 and 3.46 ± 0.05 U g^{-1} min^{-1} FW, respectively. Nano-ALA priming further enhanced GR activity under stress, with AlpPD recording the highest value (3.70 ± 0.05 U g^{-1} min^{-1} FW), followed by AlpPS (3.56 ± 0.04 U g^{-1} min^{-1} FW). These values represented increases of approximately 6.9% and 6.6% compared with NCD and NCS, respectively. Under non-stress conditions, AlpP (2.56 ± 0.04 U g^{-1} min^{-1} FW) also exhibited significantly greater GR activity than CNP and CHP.

Ascorbate peroxidase (APX)

APX showed one of the strongest responses to nano-ALA priming (Fig. 4D). Basal APX activities were low in CNP (12.03 ± 0.23 U g^{-1} min^{-1} FW) and CHP (11.96 ± 0.20 U g^{-1} min^{-1} FW). Salinity and drought stress increased APX activity to 22.34 ± 0.32 and 21.85 ± 0.26 U g^{-1} min^{-1} FW, respectively. A substantially greater response occurred in nano-ALA-primed seedlings, with AlpPS showing the highest APX activity (44.60 ± 0.40 U g^{-1} min^{-1} FW), followed by AlpPD (42.79 ± 0.38 U g^{-1} min^{-1} FW). Relative to the corresponding stress controls, nano-ALA priming increased APX activity by approximately 99.6% under salinity and 95.8% under drought. Interestingly, AlpP

also exhibited markedly elevated APX activity (32.57 ± 0.38 U g^{-1} min^{-1} FW) under non-stress conditions, indicating a strong priming-related stimulation of this enzyme.

Guaiacol peroxidase (GPX)

GPX activity was significantly influenced by stress and nano-ALA priming (Fig. 4E). CNP exhibited the lowest activity (0.58 ± 0.02 U g^{-1} min^{-1} FW), while CHP and AlpP recorded 0.63 ± 0.02 and 0.68 ± 0.02 U g^{-1} min^{-1} FW, respectively. Salinity and drought increased GPX activity to 0.77 ± 0.02 and 0.83 ± 0.02 U g^{-1} min^{-1} FW in NCS and NCD. Nano-ALA priming further increased GPX activity to 0.96 ± 0.02 U g^{-1} min^{-1} FW in AlpPS and to the maximum value of 1.07 ± 0.02 U g^{-1} min^{-1} FW in AlpPD. These increases were approximately 24.7% and 28.9%, respectively, relative to the corresponding unprimed stress controls.

Monodehydroascorbate reductase (MDHAR)

Unlike the other antioxidant enzymes, MDHAR displayed a distinct treatment-response pattern (Fig. 4F). The highest MDHAR activity was observed in AlpP (5.32 ± 0.07 U g^{-1} min^{-1} FW), which was approximately fourfold higher than CNP (1.33 ± 0.03 U g^{-1} min^{-1} FW). Stress alone reduced MDHAR activity, with NCS and NCD exhibiting the lowest values of 1.24 ± 0.02 and 1.19 ± 0.02 U g^{-1} min^{-1} FW, respectively. Nano-ALA priming substantially alleviated this decline, increasing MDHAR activity to 2.53 ± 0.04 U g^{-1} min^{-1} FW under salinity (AlpPS) and 2.37 ± 0.04 U g^{-1} min^{-1} FW under drought (AlpPD). These values corresponded to increases of approximately 104.0% and 99.2% relative to NCS and NCD, respectively, although they remained considerably below the activity observed in non-stressed AlpP seedlings.

Ionic Homeostasis and Mineral Nutrient Content

The ionic and mineral nutrient profiles of pea seedlings were significantly altered by salinity and drought stress and were further modulated by nano-ALA priming (Fig. 5A–E). In general, stress increased Na^+ accumulation and altered K^+ concentrations while reducing P, N, and Ca contents. Priming with chitosan-encapsulated ALA partially or substantially counteracted these stress-induced changes, although the magnitude of the response varied among nutrients and stress conditions.

Sodium (Na^+)

Na^+ accumulation differed significantly among treatments (Fig. 5A). Salinity stress resulted in the highest Na^+ concentration in NCS (2.07 ± 0.02 μmol g^{-1} DW), representing a 53.3% increase relative to CNP (1.35 ± 0.01 μmol g^{-1} DW). Drought stress also increased Na^+ accumulation, reaching 1.83 ± 0.03 μmol g^{-1} DW in NCD. Nano-ALA priming significantly restricted Na^+ accumulation under both stresses. Na^+ concentration decreased to 1.78 ± 0.02 μmol g^{-1} DW in AlphSP, corresponding to a 14.0% reduction compared with NCS, and to 1.68 ± 0.02 μmol g^{-1} DW in AlphDP, an 8.2% reduction compared with NCD. The lowest Na^+ concentration was observed in non-stressed AlpP (1.18 ± 0.01 μmol g^{-1} DW), which was approximately 12.6% lower than CNP, indicating that nano-ALA priming strongly influenced Na^+ accumulation even in the absence of stress.

Potassium (K^+)

K^+ concentration also varied significantly among treatments (Fig. 5B). The highest value was recorded in NCD (2.13 ± 0.01 μmol g^{-1} DW), followed by NCS (1.93 ± 0.02 μmol g^{-1} DW), representing increases of approximately 28.3% and 16.3%, respectively, relative to CNP (1.66 ± 0.02 μmol g^{-1} DW). Nano-ALA priming moderated these stress-associated increases, with K^+ concentrations declining to 1.82 ± 0.01 μmol g^{-1} DW in AlphDP and 1.73 ± 0.01 μmol g^{-1} DW in AlphSP. These values were 14.6% and 10.4% lower than those of NCD and NCS, respectively. Thus, nano-ALA priming moderated stress-induced alterations in K^+ accumulation rather than simply increasing K^+ content, contributing to a more regulated ionic status under adverse conditions.

Phosphorus (P)

P content declined significantly under both stress treatments (Fig. 5C). NCS exhibited the lowest P concentration (2.11 ± 0.01), representing a 26.5% reduction relative to CNP (2.87 ± 0.01), while NCD showed a 13.6% reduction, reaching 2.48 ± 0.01. In contrast, AlpP recorded the highest P content (3.28 ± 0.01), followed by CHP (3.06 ± 0.02). Nano-ALA priming significantly alleviated the stress-induced decline in P, increasing its content to 2.70 ± 0.01 in AlphSP and 2.93 ± 0.01 in AlphDP, corresponding to increases of approximately 28.0% and 18.1% over NCS and NCD, respectively. Notably, the P content of AlphDP was statistically comparable with that of CNP, indicating substantial restoration under drought stress.

Nitrogen (N)

Stress exposure significantly reduced N content (Fig. 5D). N concentrations decreased from 18.50 ± 0.12 in CNP to 16.53 ± 0.15 in NCS and 17.30 ± 0.06 in NCD, corresponding to reductions of approximately 10.6% and 6.5%, respectively. The highest N content was recorded in AlpP (20.30 ± 0.06), which was approximately 9.7% greater than CNP and 22.8% greater than NCS. Nano-ALA priming significantly improved N accumulation under both stresses, increasing N content to 18.00 ± 0.06 in AlphSP and 18.90 ± 0.06 in AlphDP. These values represented increases of approximately 8.9% and 9.2% relative to NCS and NCD, respectively. Importantly, AlphDP was statistically comparable with CNP, suggesting that nano-ALA priming effectively restored N status under drought stress.

Calcium (Ca)

Ca content was markedly affected by stress and priming treatments (Fig. 5E). Salinity caused the greatest decline, reducing Ca from 15.00 ± 0.12 in CNP to 12.00 ± 0.12 in NCS, equivalent to a 20.0% reduction. Drought stress decreased Ca to 13.60 ± 0.06, representing a 9.3% reduction relative to CNP. AlpP exhibited the highest Ca content (16.90 ± 0.06), followed by CHP (16.13 ± 0.18). Nano-ALA priming partially restored Ca accumulation under stress, increasing Ca to 13.10 ± 0.06 in AlphSP and 14.60 ± 0.06 in AlphDP. Relative to their respective stress controls, these values represented increases of approximately 9.2% under salinity and 7.4% under drought. The stronger recovery observed in AlphDP indicates that nano-ALA priming was particularly effective in preserving Ca nutrition under drought conditions.

Micronutrient Content

Micronutrient concentrations were significantly affected by salinity, drought, and nano-ALA priming (Fig. 6A–D). In general, both stresses reduced Fe, Zn, Mn, and Cu accumulation, whereas priming with chitosan-encapsulated ALA partially or substantially alleviated these reductions. The extent of recovery varied among individual elements and stress conditions.

Iron (Fe)

Fe content decreased significantly under salinity stress, with NCS recording the lowest value (102.00 ± 1.15) compared with CNP (119.00 ± 0.58), corresponding to a reduction of

approximately 14.3% (Fig. 6A). Drought stress also reduced Fe content to 112.00 ± 0.58, approximately 5.9% lower than CNP. In contrast, AlpP exhibited the highest Fe content (130.00 ± 0.58), representing an increase of approximately 9.2% relative to CNP. Nano-ALA priming significantly improved Fe status under both stresses, increasing Fe to 109.00 ± 0.58 in AlphSP and 117.00 ± 0.58 in AlphDP. These values corresponded to increases of approximately 6.9% and 4.5% relative to NCS and NCD, respectively. Notably, Fe content in AlphDP was statistically comparable with that of CNP, indicating substantial recovery under drought stress.

Zinc (Zn)

Zn content was significantly reduced by both salinity and drought stress (Fig. 6B). Compared with CNP (36.33 ± 0.33), Zn declined to 30.00 ± 0.58 in NCS and 34.33 ± 0.33 in NCD, representing reductions of approximately 17.4% and 5.5%, respectively. AlpP recorded the highest Zn content (42.33 ± 0.33), approximately 16.5% greater than CNP, followed by CHP (39.00 ± 0.58). Nano-ALA priming significantly improved Zn accumulation under stress, increasing Zn to 33.33 ± 0.33 in AlphSP and 38.33 ± 0.33 in AlphDP. Relative to their corresponding stress controls, these increases were approximately 11.1% under salinity and 11.7% under drought. AlphDP exhibited Zn concentrations statistically comparable with CHP, demonstrating a particularly strong recovery under drought conditions.

Manganese (Mn)

Mn content also declined in response to abiotic stress (Fig. 6C). Salinity caused the greatest reduction, decreasing Mn from 42.33 ± 0.33 in CNP to 35.33 ± 0.33 in NCS, equivalent to a 16.5% decrease. Drought reduced Mn to 39.33 ± 0.33, approximately 7.1% below CNP. The highest Mn content was observed in AlpP (48.33 ± 0.33), representing an increase of approximately 14.2% over CNP, followed by CHP (45.00 ± 0.58). Under salinity, nano-ALA priming increased Mn to 37.33 ± 0.33 in AlphSP, a significant 5.7% increase compared with NCS. Under drought, AlphDP reached 41.33 ± 0.33, approximately 5.1% higher than NCD; however, these two treatments shared the same statistical grouping, indicating that the numerical increase was not significant at $p \leq 0.05$. Thus, nano-ALA priming more clearly improved Mn retention under salinity than under drought.

Copper (Cu)

Cu content was markedly reduced under stress, particularly salinity (Fig. 6D). NCS recorded the lowest Cu concentration (4.10 ± 0.06) compared with CNP (5.30 ± 0.06), representing a reduction of approximately 22.6%. Drought stress decreased Cu to 4.90 ± 0.06, approximately 7.5% lower than CNP. AlpP exhibited the highest Cu content (6.10 ± 0.06), corresponding to an increase of approximately 15.1% relative to CNP, followed by CHP (5.70 ± 0.06). Nano-ALA priming partially restored Cu under both stress conditions, increasing its content to 4.63 ± 0.03 in AlphSP and 5.20 ± 0.06 in AlphDP. These values represented increases of approximately 12.9% and 6.1% relative to NCS and NCD, respectively. Notably, Cu content in AlphDP was statistically comparable with CNP, indicating effective recovery under drought stress.

Oxidative Stress Markers and Osmolyte Accumulation

Malondialdehyde (MDA)

Malondialdehyde (MDA) content, an indicator of lipid peroxidation, was significantly affected by both stress and priming treatments ($p \leq 0.05$). Salinity stress (NCS) increased MDA to 64.82 nmol g^{-1} FW compared with the non-primed control (CNP, 53.47 nmol g^{-1} FW), representing approximately a 21% increase. Drought stress (NCD) resulted in even higher MDA levels (≈66–74 nmol g^{-1} FW), indicating more severe membrane lipid peroxidation under water deficit conditions (Fig. 7A). Alpha-lipoic acid priming markedly reduced MDA accumulation under non-stress conditions. AlpP exhibited the lowest MDA value (36.36 nmol g^{-1} FW), representing nearly a 32% reduction compared with CNP. Under salinity, AlphSP maintained significantly lower MDA levels than NCS, although still higher than controls. Under drought, AlphDP showed elevated MDA compared to AlpP but remained statistically distinct from stress controls, indicating partial mitigation of oxidative damage.

Hydrogen Peroxide (H_2O_2)

Hydrogen peroxide levels increased significantly under stress conditions. NCS recorded 3.89 µmol g^{-1} FW, while NCD exhibited the highest H_2O_2 concentration (4.63 µmol g^{-1} FW), nearly 82% higher than CNP (2.55 µmol g^{-1} FW). This confirms enhanced reactive oxygen species (ROS) accumulation under both salinity and drought stress. AlpP showed the lowest H_2O_2 concentration (1.58 µmol g^{-1} FW), approximately 38% lower than CNP, indicating improved redox balance

under priming. AlphSP and AlphDP significantly reduced H_2O_2 compared with their respective stress controls, although values remained higher than non-stressed treatments. These results suggest that nano-ALA priming attenuated stress-induced ROS accumulation (Fig. 7B).

Electrolyte Leakage (EL)

Electrolyte leakage, a measure of membrane stability, increased markedly under stress. NCS showed EL values of 47.01%, while NCD exhibited the highest leakage (61.03%), more than double that of AlpP (25.53%). Compared to CNP (29.76%), drought stress increased EL by approximately 105%, indicating severe membrane damage (Fig. 7C). Nano-ALA priming significantly improved membrane stability. AlpP showed the lowest EL (25.53%), even lower than both control treatments. Under salinity, AlphSP reduced EL to 39.80%, significantly lower than NCS. Under drought, AlphDP decreased EL compared to NCD, although values remained elevated relative to controls.

Proline Accumulation

Proline content was significantly influenced by both stress and priming treatments. Drought stress (NCD) markedly increased proline accumulation (≈136 μmol g^{-1} DW), while salinity stress (NCS) also elevated proline compared to controls. Control treatments (CNP and CHP) exhibited the lowest proline concentrations (≈50–55 μmol g^{-1} DW) (Fig. 7D). Nano-ALA priming substantially enhanced proline accumulation. AlpP increased proline to approximately 113 μmol g^{-1} DW under non-stress conditions. Under salinity and drought, AlphSP and AlphDP showed the highest proline levels (≈234 and 251 μmol g^{-1} DW, respectively), significantly exceeding stress controls.

Gene Expression Analysis of Stress-Responsive Genes

LEA (Late Embryogenesis Abundant Protein)

LEA expression was strongly induced under stress conditions. Salinity stress (NCS) increased LEA transcript levels to 2.67-fold relative to the control (CNP, 1.11), while drought stress (NCD) elevated expression to 2.34-fold. Notably, AlphSP exhibited the highest LEA expression (3.67-fold), significantly exceeding all other treatments. AlphDP also maintained elevated LEA expression (2.44-fold), though lower than AlphSP. In contrast, non-stressed treatments (CNP, CHP,

and AlpP) showed comparatively low expression levels. These results suggest that nano-ALA priming, particularly under salinity, amplified LEA-mediated osmoprotective responses (Fig. 8A).

D2 Protein (PsbD)

Expression of the photosystem II D2 protein (PsbD) was significantly affected by treatment. CHP exhibited slightly higher expression (1.43-fold) compared to CNP (1.33-fold). Salinity stress (NCS) moderately increased PsbD expression (1.47-fold), whereas drought stress (NCD) markedly reduced it (0.98-fold), indicating impairment of photosystem stability under water deficit. AlpP enhanced PsbD expression (1.65-fold), suggesting improved photosynthetic protection under priming. AlphSP and AlphDP showed intermediate levels, indicating partial stabilization of PSII machinery under stress (Fig. 8B).

PDH45

PDH45 expression displayed the most pronounced drought-associated response. NCD significantly upregulated PDH45 (2.64-fold) relative to CNP (1.02-fold). However, AlphDP exhibited an exceptionally strong induction (5.42-fold), representing the highest expression among all treatments. Salinity stress (NCS) induced a moderate increase (1.57-fold), while AlpP and AlphSP showed intermediate levels. These findings indicate that nano-ALA priming under drought strongly activates helicase-mediated stress adaptation mechanisms (Fig. 8C).

ABR1

ABR1 expression was elevated under stress conditions. NCS (1.65-fold) and NCD (1.58-fold) significantly exceeded control levels (1.08-fold). AlphSP further enhanced ABR1 expression (1.76-fold), indicating enhanced ABA-responsive signaling under salinity with priming. AlphDP showed moderate induction (1.28-fold), while AlpP remained closer to control levels. These data suggest that nano-priming modulates ABA-associated stress signaling, particularly under salinity stress (Fig. 8D).

Aquaporin

Aquaporin transcripts were significantly upregulated under drought stress. NCD showed strong induction (2.37-fold), while AlphDP recorded the highest expression (2.76-fold), significantly exceeding all other treatments. Salinity stress induced moderate expression (1.42-fold), and AlphSP slightly increased this level. Control treatments exhibited the lowest aquaporin expression. This pattern indicates that nano-ALA priming enhances water channel regulation, particularly under drought conditions (Fig. 8E).

HSP70

HSP70 expression was strongly enhanced under salinity stress (1.84-fold) and drought stress (1.77-fold) compared with CNP (1.08-fold). AlphSP exhibited the highest HSP70 expression (1.92-fold), indicating enhanced molecular chaperone activity under salinity with priming. AlphDP also maintained elevated levels, though slightly lower than AlphSP. Non-stressed treatments showed minimal induction (Fig. 8F).

Osmotin-like Protein (OSM34)

OSM34 expression showed the most pronounced drought-associated pattern. NCD strongly induced OSM34 (3.54-fold), while AlphDP exhibited the highest expression (4.16-fold), significantly exceeding all other treatments. Salinity stress (NCS) caused only slight induction (1.34-fold). AlpP and AlphSP maintained moderate expression levels. These findings confirm that OSM34 is primarily responsive to drought stress and is strongly enhanced by nano-ALA priming (Fig. 8G).

Discussion

The present study demonstrated that seed priming with α-lipoic acid encapsulated in chitosan nanoparticles (Ch-ALA-NPs) substantially enhanced the tolerance of pea (*Pisum sativum* L.)

seedlings to salinity and drought stress through coordinated improvements in germination, antioxidant defense, membrane stability, osmotic adjustment, ionic homeostasis, mineral nutrition, and stress-responsive gene expression. These responses support the growing evidence that nanopriming can establish a physiologically prepared state before stress exposure, thereby enabling more rapid and effective activation of protective mechanisms when unfavorable conditions occur (Soni et al., 2023; Alenazi et al., 2024; Santhy et al., 2026).

Physicochemical analyses confirmed the successful incorporation of ALA into chitosan nanoparticles. ALA loading increased the hydrodynamic diameter from 112.4 to 148.7 nm and slightly increased the PDI, while the particles retained a relatively narrow size distribution. The positive zeta potential declined from +34.6 mV in Ch-NPs to +28.9 mV following ALA incorporation, most likely because ALA interacted with or partially masked the protonated amino groups of chitosan. Nevertheless, the nanoparticles maintained a positive surface charge, which is generally considered favorable for colloidal stability and interaction with negatively charged biological surfaces. Similar changes in particle size and surface charge after incorporation of bioactive molecules into chitosan nanocarriers have been widely reported and are attributed to molecular interactions within the chitosan network.

The FTIR shifts in O–H/N–H, amide I, amide II, and C–O–C bands, together with the appearance of the ALA-associated carbonyl band at 1715 cm^{-1}, provide further evidence for successful ALA incorporation and suggest hydrogen-bonding and electrostatic interactions between ALA and chitosan. The reduction in crystallite size and broadening of the XRD diffraction peak after ALA loading also indicate disruption of the ordered chitosan structure and formation of a comparatively more amorphous nanoparticle matrix. Such reduced crystallinity may facilitate hydration and diffusion of the encapsulated compound and consequently influence its release behavior.

The encapsulation efficiency of 78.4% and loading capacity of 12.6% additionally indicate effective incorporation of ALA into the chitosan matrix. Chitosan-based nanocarriers are particularly attractive for agricultural applications because of their biodegradability, biocompatibility, positive surface charge, and ability to provide controlled delivery of bioactive compounds (Soni et al., 2023; Alenazi et al., 2024). Thus, nanoencapsulation may have protected ALA against rapid degradation while facilitating its availability during seed imbibition and early seedling development.

Salinity and drought markedly impaired germination performance, as evidenced by reduced final germination percentage and germination index and increased T50 and mean germination time. These effects are consistent with the well-established inhibitory effects of osmotic stress, ionic toxicity, impaired water uptake, and oxidative damage on seed germination. By contrast, Ch-ALA-NP priming substantially improved germination under both stress conditions, while AlpP exhibited 100% germination and the shortest germination time under non-stress conditions.

Seed priming activates several pregerminative metabolic processes before radicle emergence, including DNA repair, mitochondrial activation, antioxidant metabolism, and mobilization of seed reserves. Consequently, primed seeds are generally able to resume germination more rapidly after exposure to favorable or stressful conditions. Chitosan nanoparticle priming has similarly been reported to enhance germination and seedling vigor under salinity and drought by improving water uptake, antioxidant capacity, and metabolic activation (Soni et al., 2023; Santhy et al., 2026). The present response may reflect complementary effects of chitosan and ALA. Chitosan can itself act as an elicitor of plant defense pathways, whereas ALA is a potent redox-active metabolite with antioxidant and metabolic functions. Previous studies have shown that exogenous ALA improves plant performance under salinity and drought through regulation of antioxidant metabolism, photosynthesis, osmotic adjustment, and ion homeostasis (Gorcek and Erdal, 2015; Youssef et al., 2021; Daler and Kaya, 2024; Mian et al., 2024). Encapsulation of ALA within chitosan nanoparticles may therefore provide a synergistic priming system in which the carrier improves ALA stability and delivery while simultaneously contributing its own elicitor activity.

One of the strongest effects of nano-ALA priming was the activation of antioxidant enzymes. Salinity and drought alone stimulated CAT, SOD, GR, APX, and GPX activities, indicating activation of endogenous defense mechanisms in response to increased oxidative stress. However, these activities were further enhanced in nano-ALA-primed seedlings, demonstrating a stronger antioxidant capacity. SOD represents the first major enzymatic barrier against oxidative stress by converting superoxide radicals into H_2O_2, whereas CAT, APX, and GPX subsequently detoxify H_2O_2. GR and MDHAR participate in recycling reduced glutathione and ascorbate and therefore contribute to maintenance of the cellular redox state through the ascorbate–glutathione cycle. Enhancement of these enzymes by nano-ALA priming consequently indicates activation of multiple interconnected ROS-scavenging pathways.

Similar responses have previously been reported following ALA application. In wheat seedlings exposed to salinity, ALA enhanced antioxidant enzyme activities and improved the regeneration of glutathione and ascorbate, resulting in reduced oxidative injury (Gorcek and Erdal, 2015). Likewise, ALA increased SOD, CAT, APX, and peroxidase activities in salt-stressed sorghum (Youssef et al., 2021). Enhanced antioxidant defense following ALA treatment has also been observed under drought stress in grapevine and mungbean (Daler and Kaya, 2024; Mian et al., 2024). The exceptionally strong APX response observed in AlpPS and AlpPD suggests that the ascorbate-dependent H_2O_2-scavenging pathway may represent a major component of Ch-ALA-NP-mediated stress protection. GR stimulation further supports this interpretation because glutathione regeneration is required to sustain operation of the ascorbate–glutathione cycle.

Interestingly, MDHAR showed a different response from the other antioxidant enzymes, with maximum activity in non-stressed AlpP seedlings. This finding may indicate that nano-ALA priming preconditioned the ascorbate recycling system before stress exposure. Because ALA can interact with glutathione- and ascorbate-dependent redox systems, increased MDHAR activity before stress may establish a more reduced cellular environment that allows faster antioxidant responses following stress exposure (Gorcek and Erdal, 2015).

The enhanced antioxidant capacity was accompanied by substantial reductions in oxidative damage. Both salinity and drought increased H_2O_2, MDA, and electrolyte leakage, whereas nano-ALA priming significantly reduced these parameters. Elevated H_2O_2 under stress reflects excessive ROS production, while MDA is a major product of membrane lipid peroxidation and is widely used as an indicator of oxidative membrane damage.

The simultaneous decreases in H_2O_2, MDA, and electrolyte leakage therefore demonstrate that enhanced antioxidant activity translated into effective protection of cellular membranes. ALA has previously been reported to decrease ROS accumulation and lipid peroxidation under salinity by strengthening antioxidant defense mechanisms (Gorcek and Erdal, 2015; Youssef et al., 2021). Similarly, exogenous ALA reduced MDA accumulation and electrolyte leakage in drought-stressed grapevine while enhancing CAT, SOD, and APX activities (Daler and Kaya, 2024). Chitosan nanoparticles may additionally contribute to this protective effect. Chitosan nanoparticle treatments have been shown to suppress H_2O_2 accumulation, lipid peroxidation, and electrolyte leakage in plants exposed to salinity, thereby maintaining membrane stability (Alenazi et al.,

2024). The marked reductions observed in the present study may therefore arise from combined effects of ALA-mediated redox regulation and chitosan-mediated stress elicitation.

Proline accumulation increased markedly under stress and was further enhanced by nano-ALA priming, with AlpPS and AlpPD exhibiting the greatest concentrations. Proline is an important compatible solute that contributes to osmotic adjustment, stabilization of proteins and membranes, maintenance of cellular hydration, and ROS buffering under salinity and drought.

The simultaneous occurrence of increased proline and reduced electrolyte leakage in nano-primed seedlings suggests that proline accumulation contributed to preservation of membrane integrity and cellular water balance. Similar stimulation of osmolyte accumulation following ALA application has previously been reported under salinity and drought (Gorcek and Erdal, 2015; Daler and Kaya, 2024). Mian et al. (2024) also demonstrated that ALA-mediated improvement of drought tolerance in mungbean was associated with enhanced water relations, antioxidant metabolism, and osmotic adjustment. Thus, enhanced proline accumulation in AlpPS and AlpPD appears to represent an adaptive response rather than simply a consequence of stress injury because it was accompanied by reduced oxidative damage and improved physiological performance.

A major consequence of salinity stress was excessive Na^+ accumulation. The strong increase in Na^+ under NCS is consistent with disruption of membrane selectivity and ion transport under high external salinity. Excessive Na^+ accumulation can impair enzyme activity, destabilize membranes, interfere with K^+-dependent metabolic processes, and disturb cellular ionic homeostasis.

Nano-ALA priming significantly decreased Na^+ accumulation under salinity and drought, suggesting improved regulation of ion uptake, exclusion, or compartmentation. Previous studies similarly demonstrated that ALA treatment reduced Na^+ accumulation and improved ion homeostasis in salt-stressed wheat and sorghum (Gorcek and Erdal, 2015; Youssef et al., 2021). In sorghum, these improvements were associated with modulation of salt-responsive transport systems, including HKT1-, SOS1-, and NHX-related pathways (Youssef et al., 2021). The K^+ response in the present study was more complex because the highest K^+ concentrations occurred in stressed controls. Therefore, the effect of nano-ALA priming should not be interpreted simply as increased K^+ uptake. Instead, nano-ALA moderated the stress-induced changes in K^+ concentration and produced values closer to those of non-stressed seedlings. This response may reflect improved regulation of ionic balance rather than indiscriminate ion accumulation. Such

regulation is particularly important under salinity because maintenance of appropriate cytosolic Na^+ and K^+ concentrations is more physiologically relevant than absolute accumulation of either ion. Chitosan-based treatments have also been reported to improve ion homeostasis and reduce salt-induced ionic toxicity (Soni et al., 2023; Alenazi et al., 2024).

Salinity and drought reduced P, N, and Ca concentrations, whereas nano-ALA priming substantially improved their accumulation. Nutrient deficiency under abiotic stress commonly arises from impaired root growth, decreased membrane transport, altered rhizosphere chemistry, reduced transpiration-driven nutrient movement, and competition between toxic ions and essential mineral elements.

Phosphorus is essential for ATP synthesis, phosphorylation reactions, membrane phospholipids, and nucleic acid metabolism. The pronounced decline in P under salinity therefore indicates disruption of energy and metabolic processes. Restoration of P by AlpPS and AlpPD may support improved energy availability required for antioxidant metabolism and stress recovery. Nitrogen is similarly fundamental to proteins, nucleic acids, pigments, and enzymes. Improved N accumulation following nano-ALA priming may therefore contribute to maintenance of metabolic and photosynthetic capacity. ALA-mediated enhancement of physiological and photosynthetic performance under abiotic stress has been reported in several species (Gorcek and Erdal, 2015; Youssef et al., 2021; Daler and Kaya, 2024). Calcium has both structural and signaling functions and is critically involved in membrane stabilization and stress signal transduction. The restoration of Ca in nano-ALA-primed seedlings may therefore contribute to both membrane integrity and activation of downstream defense responses. Improved Ca homeostasis following ALA treatment under salinity has similarly been reported by Youssef et al. (2021).

Salinity and drought also reduced Fe, Zn, Mn, and Cu concentrations, whereas nano-ALA priming partially restored their levels. These micronutrients are particularly important because they function as cofactors in antioxidant, photosynthetic, and respiratory processes. Fe is required for electron transport, chlorophyll metabolism, and numerous redox enzymes. Zn contributes to enzyme structure, transcriptional regulation, membrane stability, and antioxidant defense. Mn is essential for the oxygen-evolving complex of photosystem II and functions as a cofactor for several enzymes, including Mn-SOD, while Cu is required for plastocyanin, Cu/Zn-SOD, and other redox proteins.

Consequently, restoration of Fe, Zn, Mn, and Cu by Ch-ALA-NPs may have contributed to the enhanced antioxidant and photosynthetic protection observed in treated seedlings. Conversely, improved membrane integrity and root functionality resulting from reduced oxidative damage may have promoted micronutrient uptake. Thus, the antioxidant and mineral responses may form mutually reinforcing components of the overall stress-protective mechanism.

The physiological responses were accompanied by substantial changes in the expression of stress-responsive genes, demonstrating that nano-ALA priming influenced molecular signaling in addition to biochemical defense. LEA expression was strongly induced by stress and reached its maximum level in AlpPS. Late embryogenesis abundant proteins are highly hydrophilic proteins that accumulate in response to cellular dehydration and contribute to stabilization of proteins, membranes, and macromolecular structures under drought, salinity, and osmotic stress (Hernández-Sánchez et al., 2022). The increased LEA expression in nano-ALA-treated seedlings is therefore consistent with the observed improvements in osmotic adjustment and membrane protection.

PDH45 exhibited particularly strong induction under drought, with AlpPD showing the greatest expression. PDH45 is a pea DEAD-box DNA/RNA helicase implicated in abiotic stress adaptation through maintenance of nucleic acid metabolism and stress-responsive gene expression. Overexpression of PDH45 has previously enhanced drought tolerance in peanut and rice (Manjulatha et al., 2014; Sahoo et al., 2022). Its strong induction in AlpPD therefore suggests that Ch-ALA-NP priming activated molecular processes associated with drought acclimation. Aquaporin expression also increased markedly under drought and was highest in AlpPD. Aquaporins regulate transmembrane water movement, root hydraulic conductivity, cellular water relations, and responses to osmotic stress. Their expression and activity are closely regulated by drought, ABA, phosphorylation, Ca^{2+}, and ROS signaling (Patel and Mishra, 2021). Enhanced aquaporin expression may consequently contribute to improved water transport and cellular hydration in nano-ALA-primed seedlings.

OSM34 showed a similarly drought-dominant pattern. Osmotin and osmotin-like proteins are members of the PR-5 family and have important roles in osmotic adjustment and adaptation to drought and salinity (Bashir et al., 2020). The strong induction of OSM34 in AlpPD, together with markedly elevated proline accumulation, indicates coordinated activation of osmoprotective

pathways. HSP70 expression increased under both stresses and was particularly enhanced under salinity in AlpPS. HSP70 proteins act as molecular chaperones and maintain protein homeostasis by preventing stress-induced protein aggregation and facilitating protein refolding and repair (Yu et al., 2015). Their induction is therefore consistent with enhanced protection of cellular proteins in nano-ALA-treated seedlings.

ABR1 expression was also modified by nano-ALA priming, particularly under salinity. However, ABR1 should not be interpreted simply as a positive ABA-responsive regulator. ABR1 is an AP2-domain transcription factor identified as a negative regulator of ABA responsiveness and may participate in feedback regulation of ABA signaling (Pandey et al., 2005). Its increased expression under stress may therefore reflect fine regulation of ABA sensitivity rather than direct activation of the pathway.

PsbD, encoding the photosystem II D2 protein, showed contrasting responses to salinity and drought. Drought reduced its expression, whereas nano-ALA priming partially restored PsbD transcript abundance. Because the D2 protein is an essential component of the PSII reaction center, maintenance of PsbD expression may contribute to preservation of PSII integrity under oxidative stress. ALA-mediated protection of photosynthetic machinery has been reported previously under several abiotic stresses (Gorcek and Erdal, 2015; Daler and Kaya, 2024).

Taken together, the results indicate that Ch-ALA-NP priming induced a coordinated multilevel defense response rather than acting through a single biochemical pathway. Chitosan nanoparticles likely served both as a carrier for ALA and as a biological elicitor, whereas ALA contributed to redox regulation and metabolic protection. Such complementary activity could explain the greater stress tolerance observed following nano-ALA treatment compared with non-primed stressed seedlings.

A plausible sequence is that nano-ALA priming establishes an enhanced antioxidant and redox state during seed imbibition. Following exposure to salinity or drought, primed seedlings are consequently able to activate SOD, CAT, APX, GPX, GR, and related antioxidant pathways more efficiently, thereby restricting ROS accumulation and lipid peroxidation. Improved antioxidant protection preserves membrane integrity, which in turn contributes to more effective regulation of Na^+ and essential nutrients. Simultaneously, enhanced proline accumulation supports osmotic adjustment, while increased expression of LEA, PDH45, aquaporin, HSP70, OSM34, and other

stress-responsive genes strengthens cellular protection, water relations, protein stability, and stress signaling (Manjulatha et al., 2014; Yu et al., 2015; Bashir et al., 2020; Patel and Mishra, 2021; Hernández-Sánchez et al., 2022).

These integrated responses ultimately explain the improved germination and stress tolerance of Ch-ALA-NP-primed pea seedlings. The results are consistent with previous evidence demonstrating beneficial effects of ALA on redox homeostasis and abiotic stress tolerance (Gorcek and Erdal, 2015; Youssef et al., 2021; Daler and Kaya, 2024; Mian et al., 2024) and with studies showing that chitosan nanoparticle priming can enhance seedling establishment and stress adaptation (Soni et al., 2023; Alenazi et al., 2024; Santhy et al., 2026).

Nevertheless, the molecular mechanisms should be interpreted cautiously because transcript abundance does not necessarily correspond directly to protein abundance or activity. Moreover, inclusion of separate free-ALA and unloaded Ch-NP treatments in future studies would help distinguish the individual effects of ALA, the chitosan carrier, and nanoencapsulation. Further investigation of ALA release kinetics, nanoparticle uptake, tissue ALA concentrations, Na^+/K^+ ratios, AsA/DHA and GSH/GSSG redox couples, and protein-level expression of key stress markers would provide more direct mechanistic evidence. Despite these limitations, the present findings strongly support Ch-ALA-NP seed priming as a promising strategy for improving pea establishment and tolerance under salinity and drought stress.

Conclusion

The present study demonstrates that α-lipoic acid encapsulated in chitosan nanoparticles acts as an effective nano-priming agent that significantly enhances pea seedling tolerance to salinity and drought stress. Nano-ALA priming improved germination performance by accelerating metabolic activation and increasing final germination percentage, even under adverse conditions. These early advantages were closely associated with a strengthened antioxidant defense system, particularly through coordinated activation of the SOD–APX–GR cascade, which efficiently regulated reactive oxygen species and minimized oxidative damage.

Reduced accumulation of H_2O_2 and malondialdehyde, together with lower electrolyte leakage, confirmed that nano-priming preserved membrane integrity and limited lipid peroxidation under stress. In parallel, nano-ALA improved ionic homeostasis by reducing Na^+ accumulation,

maintaining a favorable Na^+/K^+ balance, and partially restoring macro- and micronutrient content. Enhanced proline accumulation and upregulation of stress-responsive genes, including LEA, aquaporin, PDH45, HSP70, and OSM34, further indicate that nano-ALA priming reprogrammed both osmotic adjustment and molecular stress signaling pathways. These physiological, biochemical, and transcriptional responses suggest that nano-ALA priming functions as a redox-modulating strategy that prepares seedlings for oxidative and osmotic stress. By integrating antioxidant reinforcement, membrane stabilization, ionic regulation, and stress-related gene activation, chitosan-encapsulated α-lipoic acid offers a promising and sustainable approach for improving early-stage stress tolerance in legumes. Future studies should explore field-level validation and long-term growth impacts to fully assess its agronomic potential.

Author contributions

Ibtisam A. M. Alghabban: Conceptualization, methodology, investigation, data curation, formal analysis, writing—original draft, and writing—review and editing. The author read and approved the final manuscript.

Funding declaration

No funding

References

Aebi H (1984) [13] Catalase in vitro. In: Methods in enzymology, vol 105. Elsevier, pp 121-126

Ahanger MA, Tomar NS, Tittal M, Argal S, Agarwal R (2017) Plant growth under water/salt stress: ROS production; antioxidants and significance of added potassium under such conditions. Physiology and Molecular Biology of Plants 23 (4):731-744

Allen LB, Siitonen PH, Thompson Jr HC (1998) Determination of copper, lead, and nickel in edible oils by plasma and furnace atomic spectroscopies. Journal of the American Oil Chemists' Society 75 (4):477-481

Aqaei P, Weria W, Marjan D, Javad R, and Struik PC (2020) Response of maize (Zea mays L.) to potassium nano-silica application under drought stress. Journal of Plant Nutrition 43 (9):1205-1216. doi:10.1080/01904167.2020.1727508

Arrigoni O, Dipierro S, Borraccino G (1981) Ascorbate free radical reductase, a key enzyme of the ascorbic acid system. FEBS letters 125 (2):242-244

Bates LS, Waldren R, Teare I (1973) Rapid determination of free proline for water-stress studies. Plant and soil 39:205-207

Beauchamp C, Fridovich I (1971) Superoxide dismutase: improved assays and an assay applicable to acrylamide gels. Anal Biochem 44 (1):276-287. doi:10.1016/0003-2697(71)90370-8

Bradford MM (1976) A rapid and sensitive method for the quantitation of microgram quantities of protein utilizing the principle of protein-dye binding. Analytical Biochemistry 72 (1):248-254. doi:https://doi.org/10.1016/0003-2697(76)90527-3

Bremner J (1965) Total nitrogen. Methods of soil analysis: part 2 chemical and microbiological properties 9:1149-1178

Chance B, Maehly A (1955) [136] Assay of catalases and peroxidases.

Dionisio-Sese ML, Tobita S (1998) Antioxidant responses of rice seedlings to salinity stress. Plant science 135 (1):1-9

El-Beltagi HS, Mohamed HI (2013) Reactive oxygen species, lipid peroxidation and antioxidative defense mechanism. Notulae Botanicae Horti Agrobotanici Cluj-Napoca 41 (1):44-57

Ellis R, Roberts E (1981) An investigation into the possible effects of ripeness and repeated threshing on barley seed longevity under six different storage environments. Annals of Botany 48 (1):93-96

Foyer CH, Halliwell B (1976) The presence of glutathione and glutathione reductase in chloroplasts: a proposed role in ascorbic acid metabolism. Planta 133:21-25

Heath RL, Packer L (1968) Photoperoxidation in isolated chloroplasts: I. Kinetics and stoichiometry of fatty acid peroxidation. Archives of biochemistry and biophysics 125 (1):189-198

Jin T, Liu T, Lam E, Moores A (2021) Chitin and chitosan on the nanoscale. Nanoscale Horizons 6 (7):505-542

Livak KJ, Schmittgen TD (2001) Analysis of relative gene expression data using real-time quantitative PCR and the $2^{-\Delta\Delta CT}$ method. methods 25 (4):402-408

Manvelian J, Weisany W, Tahir NA-r, Jabbari H, Diyanat M (2021) Physiological and biochemical response of safflower (Carthamus tinctorius L.) cultivars to zinc application under drought stress. Industrial Crops and Products 172:114069. doi:https://doi.org/10.1016/j.indcrop.2021.114069

Marthandan V, Geetha R, Kumutha K, Renganathan VG, Karthikeyan A, Ramalingam J (2020) Seed priming: a feasible strategy to enhance drought tolerance in crop plants. International journal of molecular sciences 21 (21):8258

Murphy J, Riley JP (1962) A modified single solution method for the determination of phosphate in natural waters. Analytica chimica acta 27:31-36

Nakano Y, Asada K (1981) Hydrogen peroxide is scavenged by ascorbate-specific peroxidase in spinach chloroplasts. Plant and cell physiology 22 (5):867-880

Nandini T, Sudhalakshmi C, Sivakumar K, Parameswari E, Thangamani C (2025) A review-chitosan nanoparticles towards enhancing nutrient use efficiency in crops. International Journal of Biological Macromolecules 306:141433

Pratt PF, Chapman HD (1961) Gains and losses of mineral elements in an irrigated soil during a 20-year lysimeter investigation.

Quester K, Rodríguez-González S, González-Dávalos L, Lozano-Flores C, González-Gallardo A, Zapiain-Merino SJ, Shimada A, Mora O, Vazquez-Duhalt R (2022) Chitosan Nanoparticles Containing Lipoic Acid with Antioxidant Properties as a Potential Nutritional Supplement. Animals 12 (4):417

Rao MJ, Duan M, Zhou C, Jiao J, Cheng P, Yang L, Wei W, Shen Q, Ji P, Yang Y (2025) Antioxidant defense system in plants: reactive oxygen species production, signaling, and scavenging during abiotic stress-induced oxidative damage. Horticulturae 11 (5):477

Sackey OK, Feng N, Mohammed YZ, Dzou CF, Zheng D, Zhao L, Shen X (2025) A comprehensive review on rice responses and tolerance to salt stress. Frontiers in Plant Science 16:1561280

Sharma A, Sharma P, Kumar R, Sharma V, Bhardwaj R, Sharma I (2021) Role of reactive oxygen species in the regulation of abiotic stress tolerance in legumes. In: Abiotic stress and legumes. Elsevier, pp 217-243

Soufiani SP, Yousefi S, Honarvar M, Weisany W, Asadi G (2025) Polyvinyl alcohol films incorporating cellulose nanocrystals, chitosan, and mesoporous silica nanoparticles for enhanced stability and controlled release of beet extracts. Carbohydrate Polymer Technologies and Applications 10:100740. doi:https://doi.org/10.1016/j.carpta.2025.100740

Tripathi AK, Ray AK, Mishra SK, Bishen SM, Mishra H, Khurana A (2023) Molecular and therapeutic insights of alpha-lipoic acid as a potential molecule for disease prevention. Revista brasileira de farmacognosia 33 (2):272-287

Velikova V, Yordanov I, Edreva A (2000) Oxidative stress and some antioxidant systems in acid rain-treated bean plants: protective role of exogenous polyamines. Plant science 151 (1):59-66

Wang L, Cheng C, Yu X, Guo L, Wan X, Xu J, Xiang X, Yang J, Kang J, Deng Q (2025) Conversion of α-linolenic acid into n-3 long-chain polyunsaturated fatty acids: Bioavailability and dietary regulation. Critical Reviews in Food Science and Nutrition 65 (29):6470-6502

Weisany W, Khosropour E (2023) Chapter 8 - Engineered nanomaterials in crop plants drought stress management. In: Husen A (ed) Engineered Nanomaterials for Sustainable Agricultural Production, Soil Improvement and Stress Management. Academic Press, pp 183-204. doi:https://doi.org/10.1016/B978-0-323-91933-3.00005-2

Weisany W, Razmi J, Eshaghabadi AH, Pashang D (2024) Silicon Nanoparticles (SiNP): A Novel and Sustainable Strategy for Mitigating Environmental Stresses in Plants. Journal of Soil Science and Plant Nutrition 24 (2):2167-2191. doi:10.1007/s42729-024-01790-1

Alenazi MM, El-Ebidy AM, El-Shehaby OA, Seleiman MF, Aldhuwaib KJ, Abdel-Aziz HMM (2024). Chitosan and chitosan nanoparticles differentially alleviate salinity stress in *Phaseolus vulgaris* L. plants. *Plants* 13, 398. doi: 10.3390/plants13030398. PubMed

Bashir MA, Silvestri C, Ahmad T, Hafiz IA, Abbasi NA, Manzoor A, Cristofori V, Rugini E (2020). Osmotin: A cationic protein leads to improve biotic and abiotic stress tolerance in plants. *Plants* 9, 992. doi: 10.3390/plants9080992. PubMed

Daler S, Kaya O (2024). Exogenous alpha-lipoic acid treatments reduce the oxidative damage caused by drought stress in two grapevine rootstocks. *Physiologia Plantarum* 176, e14437. doi: 10.1111/ppl.14437. Wiley Online Library

Gorcek Z, Erdal S (2015). Lipoic acid mitigates oxidative stress and recovers metabolic distortions in salt-stressed wheat seedlings by modulating ion homeostasis, the osmo-regulator level and antioxidant system. *Journal of the Science of Food and Agriculture* 95, 2811–2817. doi: 10.1002/jsfa.7020. PubMed

Hernández-Sánchez IE, Maruri-López I, Martinez-Martinez C, Janis B, Jiménez-Bremont JF, Covarrubias AA, Menze MA, Graether SP, Thalhammer A (2022). LEAfing through literature: Late embryogenesis abundant proteins coming of age—achievements and perspectives. *Journal of Experimental Botany* 73, 6525–6546. doi: 10.1093/jxb/erac293. PubMed

Manjulatha M, Sreevathsa R, Kumar AM, Sudhakar C, Prasad TG, Tuteja N, Udayakumar M (2014). Overexpression of a pea DNA helicase (PDH45) in peanut (*Arachis hypogaea* L.) confers improvement of cellular level tolerance and productivity under drought stress. *Molecular Biotechnology* 56, 111–125. doi: 10.1007/s12033-013-9687-z. PubMed

Mian NH, Azeem M, Ali Q, Mahmood S, Akram MS (2024). Alpha lipoic acid mitigates adverse impacts of drought stress on growth and yield of mungbean: Photosynthetic pigments, and antioxidative defense mechanism. *PeerJ* 12, e17191. doi: 10.7717/peerj.17191. PubMed Central (PMC)

Pandey GK, Grant JJ, Cheong YH, Kim BG, Li L, Luan S (2005). ABR1, an APETALA2-domain transcription factor that functions as a repressor of ABA response in Arabidopsis. *Plant Physiology* 139, 1185–1193. doi: 10.1104/pp.105.066324. PubMed

Patel J, Mishra A (2021). Plant aquaporins alleviate drought tolerance in plants by modulating cellular biochemistry, root architecture, and photosynthesis. *Physiologia Plantarum* 172, 1030–1044. doi: 10.1111/ppl.13324. PubMed

Sahoo RK, Chandan RK, Swain DM, Tuteja N, Jha G (2022). Heterologous overexpression of PDH45 gene of pea provides tolerance against sheath blight disease and drought stress in rice. *Plant Physiology and Biochemistry* 186, 242–251. doi: 10.1016/j.plaphy.2022.07.018. ScienceDirect

Santhy V, Dhakade P, Paul D, Kumar R, Meshram A, Mahajan S, Waghmare VN (2026). Seed priming with chitosan nanoparticles improved seed vigour parameters and antioxidant enzyme kinetics under polyethylene glycol (PEG)-induced drought stress in cotton. *BMC Plant Biology*. doi: 10.1186/s12870-026-09552-0. Springer

Soni AT, Rookes JE, Arya SS (2023). Chitosan nanoparticles as seed priming agents to alleviate salinity stress in rice (*Oryza sativa* L.) seedlings. *Polysaccharides* 4, 129–141. doi: 10.3390/polysaccharides4020010. MDPI

Youssef MHM, Raafat A, Abou El-Yazied A, Selim S, Azab E, Khojah E, El Nahhas N, Ibrahim MFM (2021). Exogenous application of alpha-lipoic acid mitigates salt-induced oxidative damage in sorghum plants through regulation growth, leaf pigments, ionic homeostasis, antioxidant enzymes, and expression of salt stress responsive genes. *Plants* 10, 2519. doi: 10.3390/plants10112519. PubMed

Yu A, Li P, Tang T, Wang J, Chen Y, Liu L (2015). Roles of Hsp70s in stress responses of microorganisms, plants, and animals. *BioMed Research International* 2015, 510319. doi: 10.1155/2015/510319.

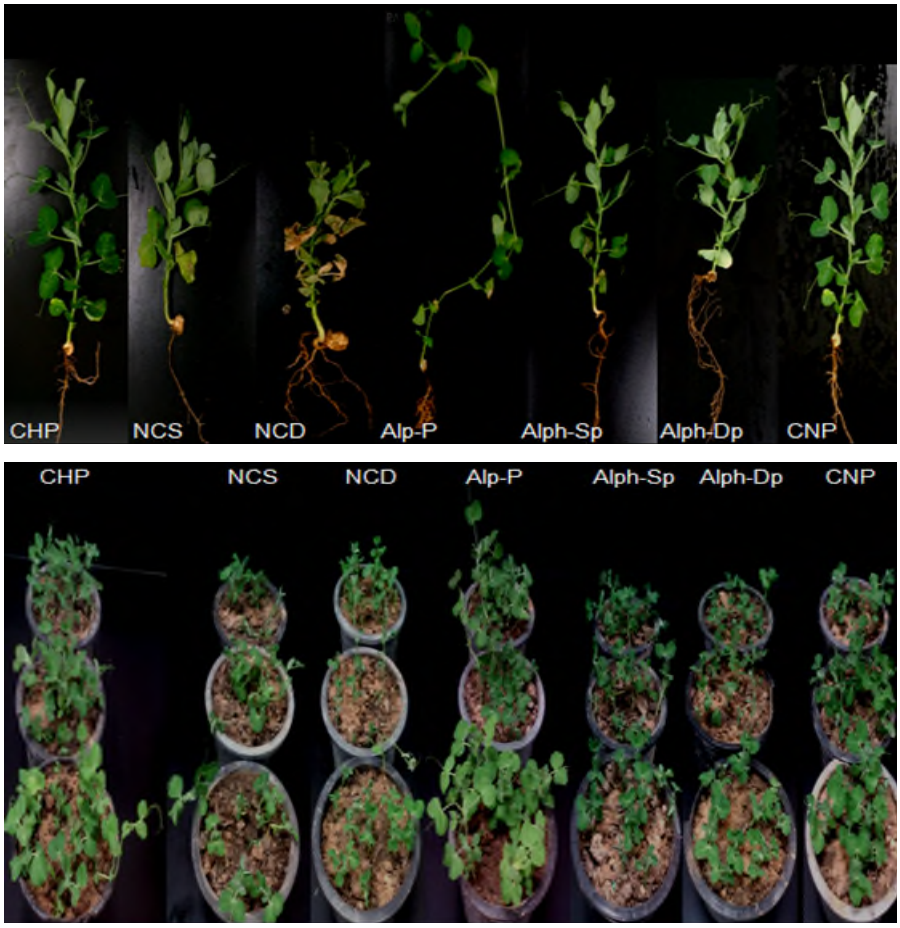

Figure 1. Experimental design and treatment groups used in the pea seed-priming study. CHP, control hydroprimed; NCS, negative control under salinity stress; NCD, negative control under drought stress; Alp-P, α-lipoic acid encapsulated in chitosan nanoparticles (nano-ALA) priming under non-stress conditions; Alph-Sp, nano-ALA priming under salinity stress; Alph-Dp, nano-ALA priming under drought stress; CNP, control non-primed dry seeds.

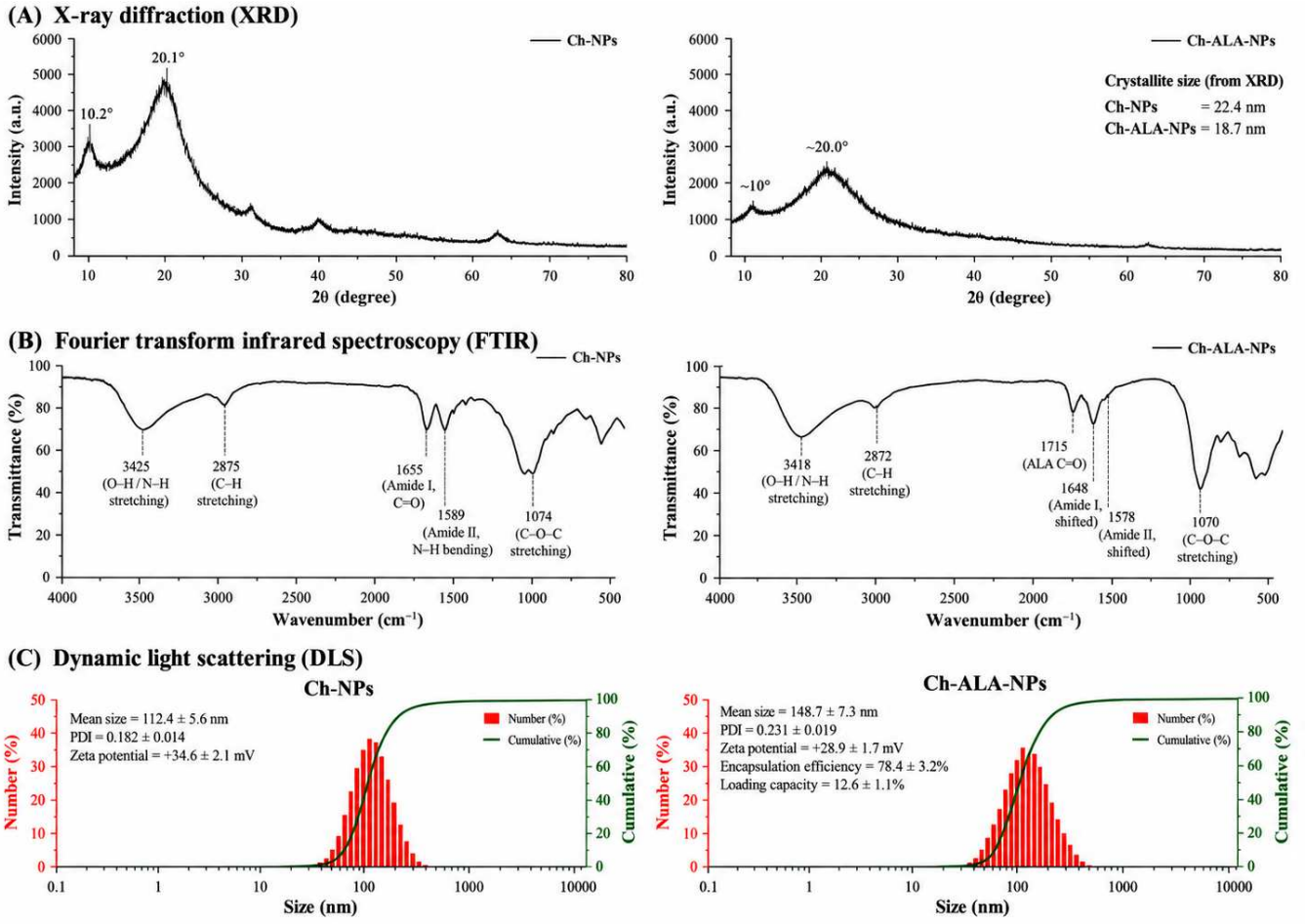

Figure 2. Physicochemical characterization of Ch-NPs and Ch-ALA-NPs: (A) XRD patterns showing reduced crystallinity after ALA loading; (B) FTIR spectra confirming interactions between ALA and chitosan; and (C) DLS profiles showing increased particle size after ALA encapsulation. Ch-ALA-NPs exhibited a mean size of 148.7 ± 7.3 nm, PDI of 0.231 ± 0.019, zeta potential of +28.9 ± 1.7 mV, encapsulation efficiency of 78.4 ± 3.2%, and loading capacity of 12.6 ± 1.1%.

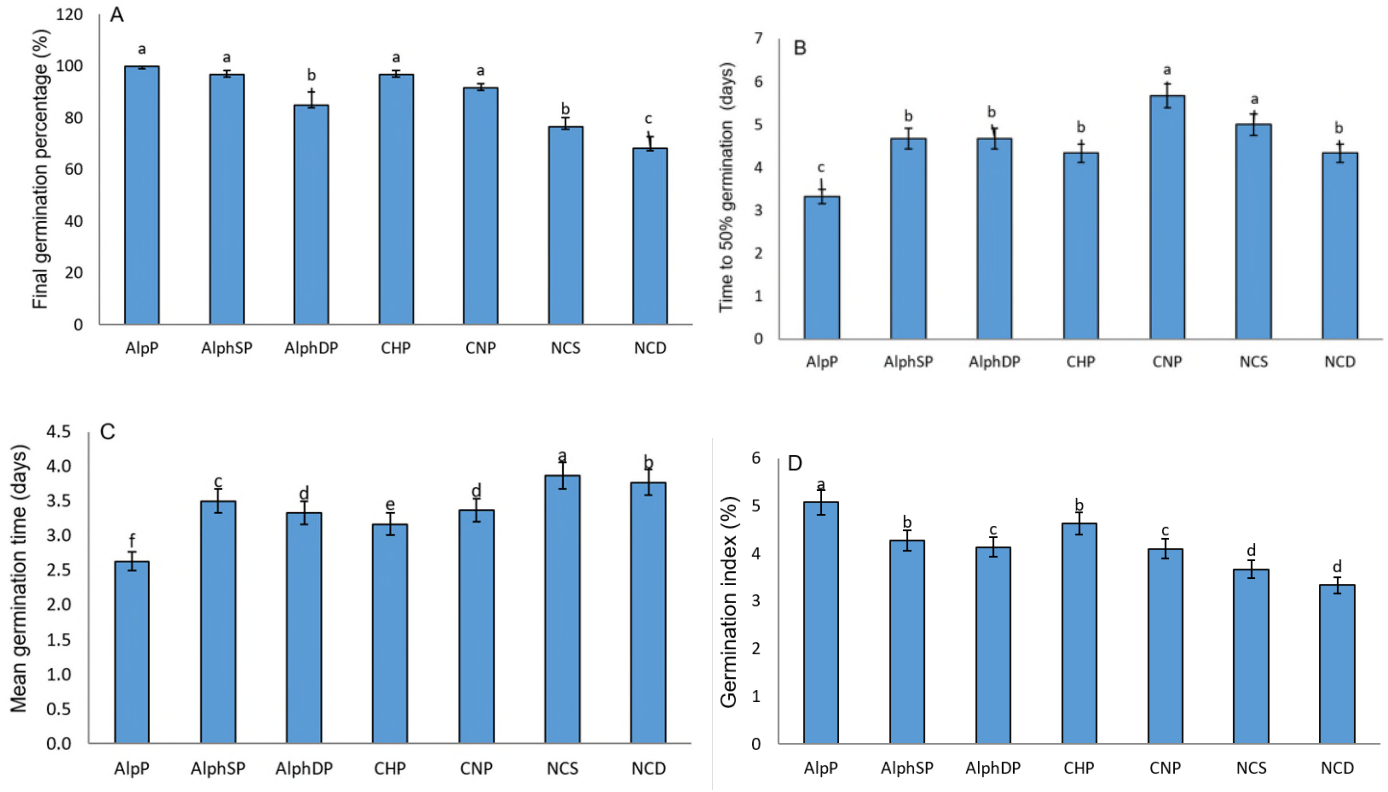

Figure 3. Effects of nano-priming and stress treatments on germination performance of pea (*Pisum sativum* L.) seedlings: (A) final germination percentage (FGP), (B) time to 50% germination (T50), (C) mean germination time (MGT), and (D) germination index (GI). Treatments included: CNP, non-primed dry seeds (control); CHP, hydroprimed control; NCS, non-primed seeds under salinity stress; NCD, non-primed seeds under drought stress; AlpP, α-lipoic acid encapsulated in chitosan nanoparticles (nano-ALA) priming without stress; AlpPS, nano-ALA priming under salinity stress; and AlpPD, nano-ALA priming under drought stress. Values are presented as means ± standard error (SE) of three replicates. Different lowercase letters above the bars indicate significant differences among treatments according to the LSD test at $p \leq 0.05$.

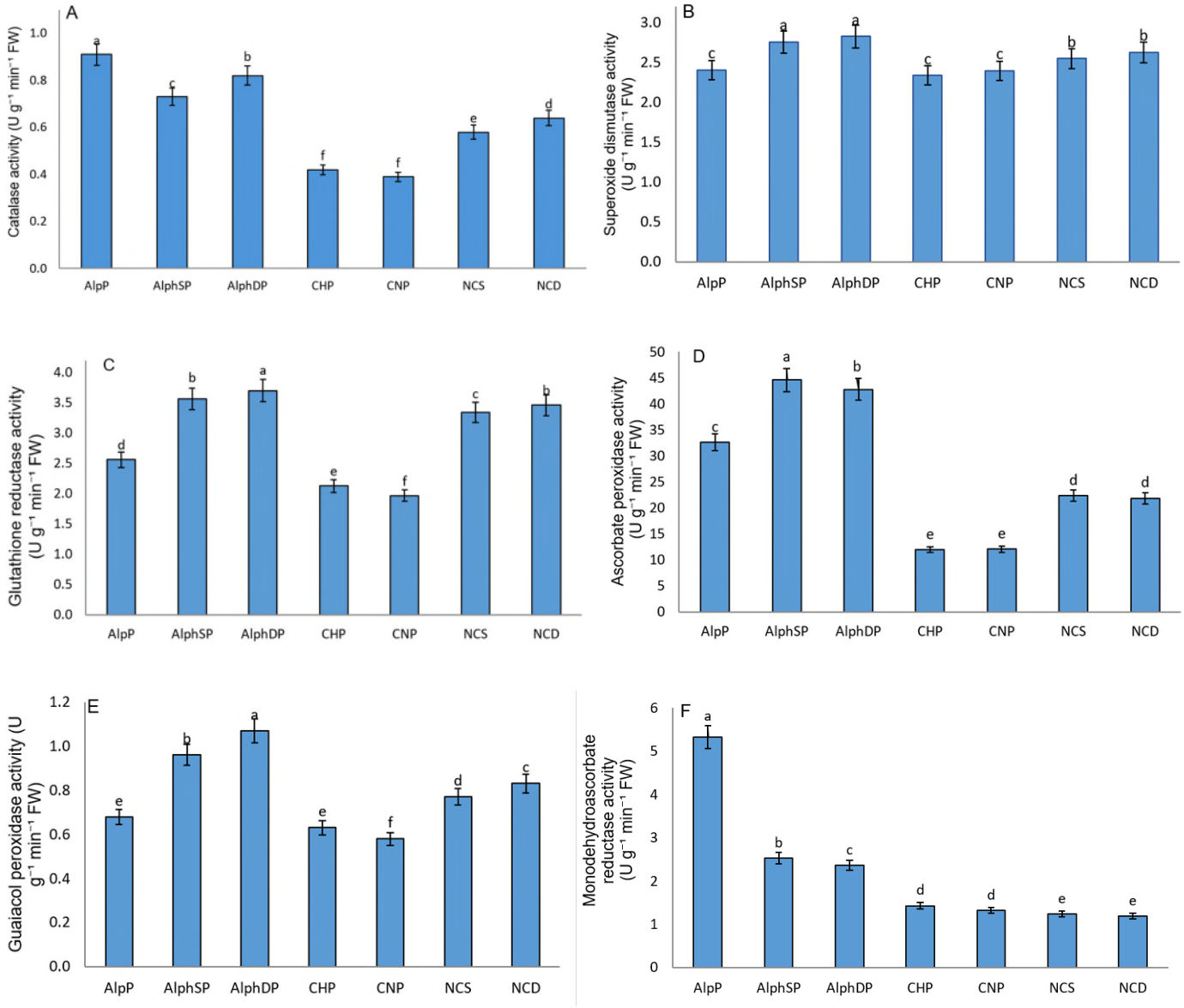

Figure 4. Effects of nano-priming and stress treatments on antioxidant enzyme activities in pea (*Pisum sativum* L.) seedlings: (A) catalase (CAT), (B) superoxide dismutase (SOD), (C) glutathione reductase (GR), (D) ascorbate peroxidase (APX), (E) guaiacol peroxidase (GPX), and (F) monodehydroascorbate reductase (MDHAR). Treatments included: CNP, non-primed dry seeds (control); CHP, hydroprimed control; NCS, non-primed seeds under salinity stress; NCD, non-primed seeds under drought stress; AlpP, α-lipoic acid encapsulated in chitosan nanoparticles (nano-ALA) priming without stress; AlpPS, nano-ALA priming under salinity stress; and AlpPD, nano-ALA priming under drought stress. Values are presented as means ± standard error (SE) of three replicates. Different lowercase letters above the bars indicate significant differences among treatments according to the LSD test at $p \leq 0.05$.

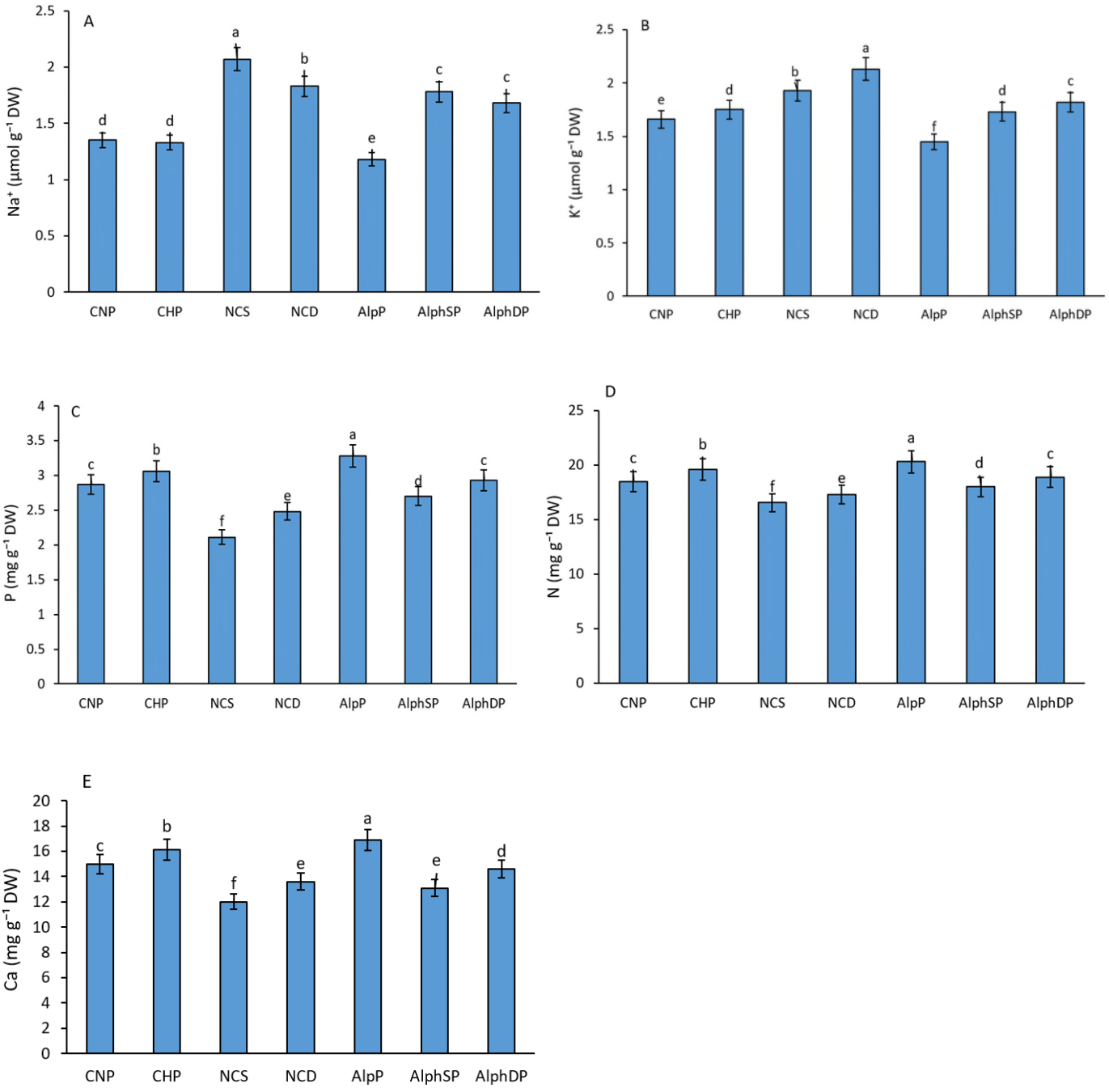

Figure 5. Effects of nano-priming and stress treatments on ionic balance and macronutrient content in pea (*Pisum sativum* L.) seedlings: (A) sodium (Na^+), (B) potassium (K^+), (C) phosphorus (P), (D) nitrogen (N), and (E) calcium (Ca). Treatments included: CNP, non-primed dry seeds (control); CHP, hydroprimed control; NCS, non-primed seeds under salinity stress; NCD, non-primed seeds under drought stress; AlpP, α-lipoic acid encapsulated in chitosan nanoparticles (nano-ALA) priming without stress; AlpPS, nano-ALA priming under salinity stress; and AlpPD, nano-ALA priming under drought stress. Values are presented as means ± standard error (SE) of three replicates. Different lowercase letters above the bars indicate significant differences among treatments according to the LSD test at $p \leq 0.05$.

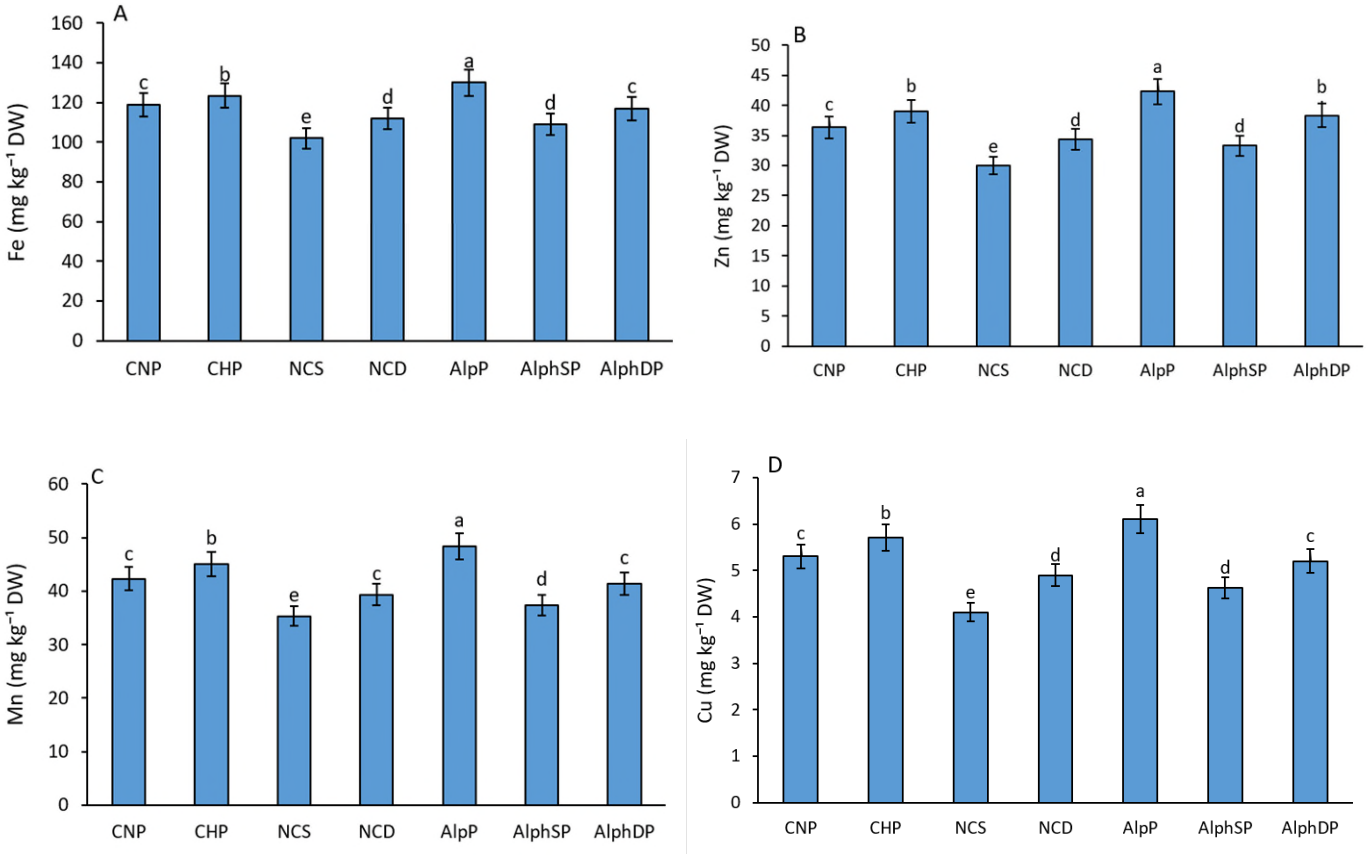

Figure 6. Effects of nano-priming and stress treatments on micronutrient content in pea (*Pisum sativum* L.) seedlings: (A) iron (Fe), (B) zinc (Zn), (C) manganese (Mn), and (D) copper (Cu). Treatments included: CNP, non-primed dry seeds (control); CHP, hydroprimed control; NCS, non-primed seeds under salinity stress; NCD, non-primed seeds under drought stress; AlpP, α-lipoic acid encapsulated in chitosan nanoparticles (nano-ALA) priming without stress; AlpPS, nano-ALA priming under salinity stress; and AlpPD, nano-ALA priming under drought stress. Values are presented as means ± standard error (SE) of three replicates. Different lowercase letters above the bars indicate significant differences among treatments according to the LSD test at $p \leq 0.05$.

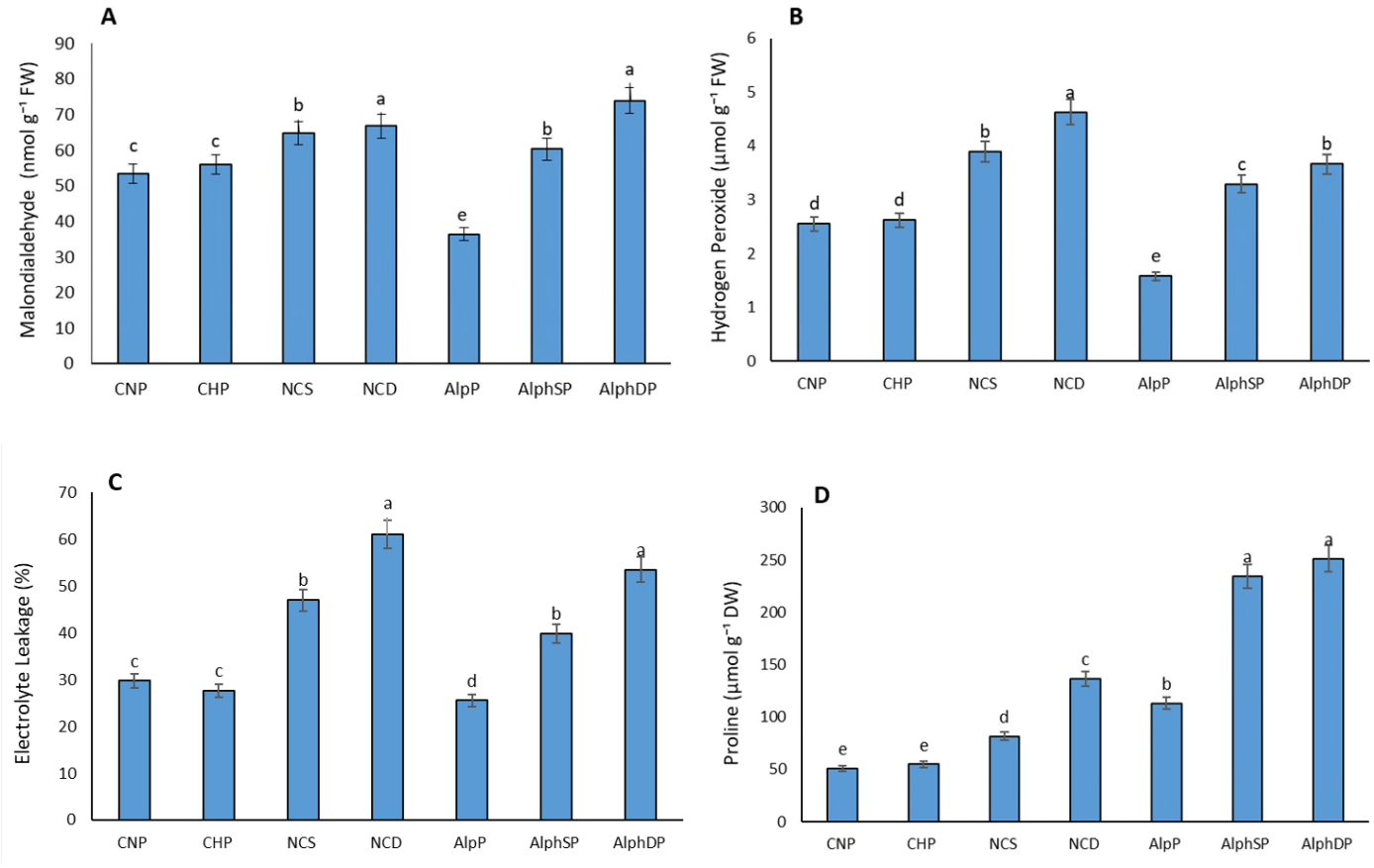

Figure 7. Effects of nano-priming and stress treatments on (A) malondialdehyde (MDA), (B) hydrogen peroxide (H_2O_2), (C) electrolyte leakage (EL), and (D) proline content in pea (*Pisum sativum* L.) seedlings under salinity and drought stress conditions. Treatments included: CNP, non-primed dry seeds (control); CHP, hydroprimed control; NCS, non-primed seeds under salinity stress; NCD, non-primed seeds under drought stress; AlpP, α-lipoic acid encapsulated in chitosan nanoparticles (nano-ALA) priming without stress; AlpPS, nano-ALA priming under salinity stress; and AlpPD, nano-ALA priming under drought stress. Values are presented as means ± standard error (SE) of three replicates. Different lowercase letters above the bars indicate significant differences among treatments according to the LSD test at $p \leq 0.05$.

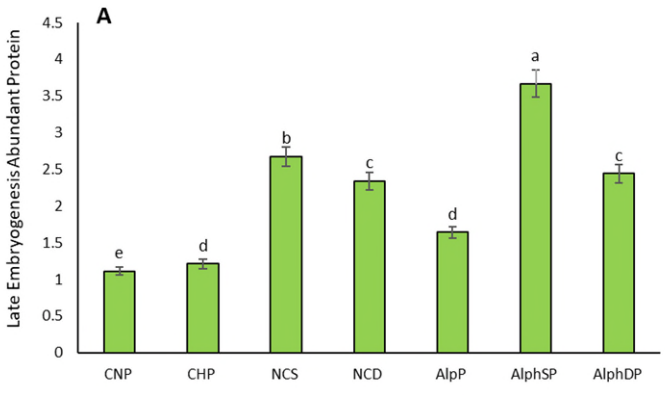
A
Late Embryogenesis Abundant Protein
4.5
4
3.5
3
2.5
2
1.5
1
0.5
0
e
d
b
c
d
a
c
CNP
CHP
NCS
NCD
AlpP
AlphSP
AlphDP

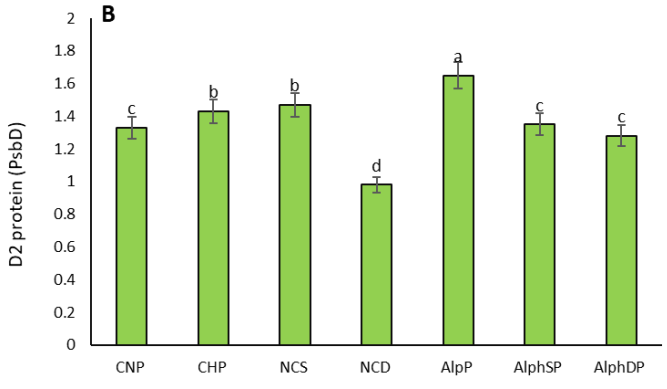
B
D2 protein (PsbD)
2
1.8
1.6
1.4
1.2
1
0.8
0.6
0.4
0.2
0
c
b
b
d
a
c
c
CNP
CHP
NCS
NCD
AlpP
AlphSP
AlphDP

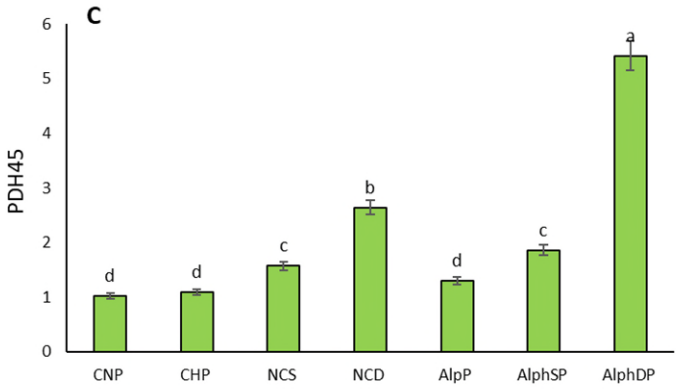
C
PDH45
6
5
4
3
2
1
0
d
d
c
b
d
c
a
CNP
CHP
NCS
NCD
AlpP
AlphSP
AlphDP

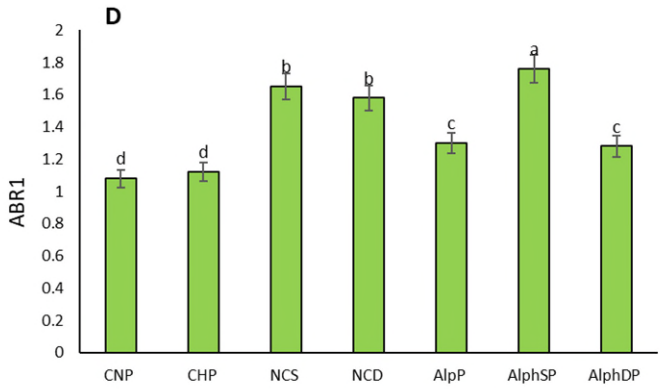
D
ABR1
2
1.8
1.6
1.4
1.2
1
0.8
0.6
0.4
0.2
0
d
d
b
b
c
a
c
CNP
CHP
NCS
NCD
AlpP
AlphSP
AlphDP

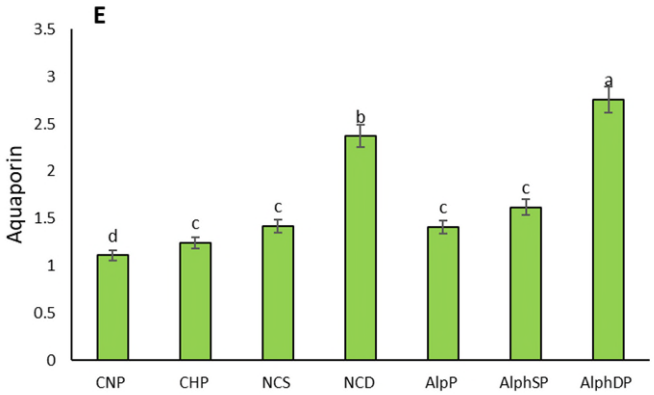
E
Aquaporin
3.5
3
2.5
2
1.5
1
0.5
0
d
c
c
b
c
c
a
CNP
CHP
NCS
NCD
AlpP
AlphSP
AlphDP

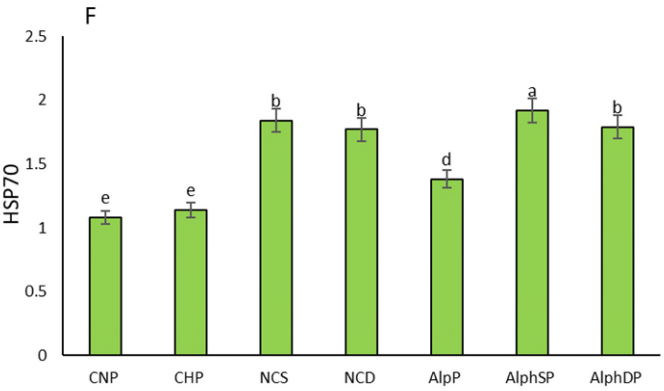
F
HSP70
2.5
2
1.5
1
0.5
0
e
e
b
b
d
a
b
CNP
CHP
NCS
NCD
AlpP
AlphSP
AlphDP

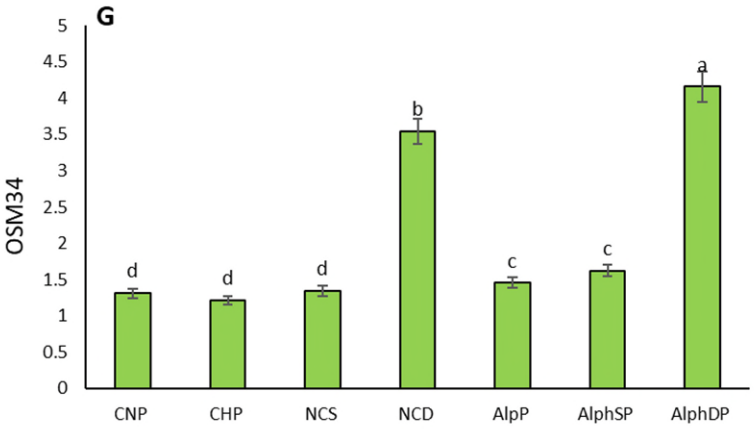
G
OSM34
5
4.5
4
3.5
3
2.5
2
1.5
1
0.5
0
d
d
d
b
c
c
a
CNP
CHP
NCS
NCD
AlpP
AlphSP
AlphDP

Figure 8. Effects of nano-priming and stress treatments on the relative expression levels of (A) *LEA* (Late Embryogenesis Abundant protein), (B) *PsbD* (D2 protein), (C) *PDH45*, (D) *ABR1*, (E) aquaporin, (F) *HSP70*, and (G) *OSM34* (osmotin-like protein) genes in pea (*Pisum sativum* L.) seedlings under salinity and drought stress conditions. Treatments included: CNP, non-primed dry seeds (control); CHP, hydroprimed control; NCS, non-primed seeds under salinity stress; NCD, non-primed seeds under drought stress; AlpP, α-lipoic acid encapsulated in chitosan nanoparticles (nano-ALA) priming without stress; AlpPS, nano-ALA priming under salinity stress; and AlpPD, nano-ALA priming under drought stress. Data represent means ± standard error (SE) of three biological replicates. Different lowercase letters above the bars indicate statistically significant differences among treatments according to the LSD test at $p \leq 0.05$.

Supplementary Files

This is a list of supplementary files associated with this preprint. Click to download.

- Suplement.docx